1 Overview

1.1 INTRODUCTION

The fundamental physics of the interactions between incident particles and target atoms provides the underlying science for ion beam analysis. These interparticle interactions depend on many parameters, including ion velocity and energy, ion and atom size, atomic number and mass, and the distance of closest approach between ion and atoms in the solid. Interactions include scattering, inner-shell ionization, and nuclear reactions. Emission products from these interactions are used to derive information on material composition and structure and provide the basis for *elemental* ion beam analysis. Other interactions control the slowing down of the ion (energy loss) and perturb its trajectory (multiple scattering) and, more importantly, bring to the methods of ion beam analysis a unique capability for deriving depth information without physically removing/sputtering the surface target material and provide the basis for ion beam *depth profiling*. The fundamental details about the interactions between incident ions and target atoms are presented in Chapters 2–9, while the applications of ion beam analysis will be covered in Chapters 10–15. Some common parameters and data tables are included in Appendices at the end of the book.

1.2 ATOMIC AND PLANAR DENSITIES

The natural unit of composition in ion beam analysis is areal density. To have a better sense of this it helps to know the atomic density, interplanar distance between planes, and the number of atoms per square

centimeter on a given plane of a material. In cubic systems with an atomic density of N atoms per cubic centimeter, the crystal lattice parameter, a_c, is given by

$$a_c = \left(\frac{\text{atoms/unit cell}}{N} \right)^{1/3} \tag{1.1}$$

where, for systems with one atom per lattice point, there are four atoms per unit cell for a face-centered cubic lattice (Al, Cu, Ag, Au, Pd, Pt), two for a body-centered cubic lattice (V, Fe, W), and eight for the common semiconductors like germanium (Ge) and silicon (Si), which have the diamond cubic structure. Aluminum has an atomic density of 6.02×10^{22} atoms/cm^3, so that the lattice parameter is

$$a_c = \left(\frac{4}{6.02 \times 10^{22}} \right)^{1/3} = 4.05 \times 10^{-8}\,\text{cm} \tag{1.2}$$

The atomic volume can be calculated without the use of crystallography. The atomic density N of atoms per cubic centimeter is given by

$$N = \frac{N_A}{A}\rho \tag{1.3}$$

where N_A is Avogadro's number, ρ is the mass density in grams per cubic centimeter, and A is the atomic mass number. Taking Al as an example, where ρ is 2.7 g/cm^3 and A is 27, the atomic density is $N = (6.02 \times 10^{23} \times 2.70)/27 = 6.02 \times 10^{22}$ atoms/cm^3. The semiconductors Ge and Si have atomic densities of about 4.4×10^{22} and 5.0×10^{22} atoms/cm^3, respectively. Metals such as Co, Ni, and Cu have densities of about 9×10^{22} atoms/cm^3. The volume Ω_v occupied by an atom is given by

$$\Omega_V = \frac{1}{N} \tag{1.4}$$

with a typical value of 20×10^{-24} cm^3.

The average areal density of a monolayer, N_s atoms/cm^2, also can be estimated without the use of crystallography by taking the atomic density N to the 2/3 power:

$$N_S \cong N^{2/3} \tag{1.5}$$

Equation (1.5) gives the average areal density of one monolayer for a material with an atomic density N. Based on this equation, the average areal density N_s for Al is approximately 1.54×10^{15} atoms/cm^2.

1.3 ENERGY AND PARTICLES

In the SI (or MKS) system of units, the joule (J) is a unit of energy, but the electron volt (eV) is the traditional unit used in ion-solid interactions. We can define 1 eV as the kinetic energy gained by an electron accelerated through a potential difference of 1 V. The charge on the electron is 1.602×10^{-19} C, and a joule is a coulomb-volt, so that the relationship between these units is given by

$$1\ \text{eV} = 1.602 \times 10^{-19}\ \text{J} \tag{1.6}$$

Commonly used multiples of the electron volt are the kiloelectron volt (keV or 10^3 eV) and megaelectron volt (MeV or 10^6 eV).

In ion–solid interactions it is convenient to use centimeter–gram–second (cgs) units rather than SI units in relations involving the charge on the electron. The usefulness of cgs units is clear when considering the Coulomb force between two charged particles with Z_1 and Z_2 units of electronic charge separated by a distance r,

$$F = k_c \frac{Z_1 Z_2 e^2}{r^2} \tag{1.7}$$

where the Coulomb law constant $k_c = \frac{1}{4\pi\varepsilon_0} = 8.988 \times 10^9$ m/F in the SI system (where 1 farad ≡ 1 ampere sec./volt) and is equal to unity in the cgs system.

The conversion factor follows from

$$e^2 k_c = (1.6 \times 10^{-19}\ \text{C})^2 \times 8.988 \times 10^9\ \text{m/F} = 2.3 \times 10^{-28}\ \text{C}^2\ \text{m/F}$$

The conversions 1 coulomb ≡ 1 ampère sec. and 1 joule ≡ 1 coulomb-volt lead to the units of the farad:

$$1\ \text{farad} \equiv 1\ \text{ampère sec. per volt}$$

so that

$$\frac{1\text{C}^2\text{m}}{\text{F}} \equiv \frac{1\text{C}^2\ \text{Vm}}{\text{As}} \equiv 1\text{J m} \equiv 10^9\ \text{J nm} \equiv \frac{10^9\ \text{J nm}}{\left(1.6 \times 10^{-19}\ \text{J/eV}\right)} = \frac{10^{28}}{1.6}\ \text{eV nm}$$

and

$$e^2 k_c = 2.31 \times 10^{-28} \frac{\text{C}^2\text{m}}{\text{F}} = \frac{2.31}{1.6}\ \text{eV nm} = 1.44\ \text{eV nm}$$

In this book we will follow the cgs units for e^2 with $k_c = 1$, so that

$$e^2 = 1.44 \text{ eV nm} \tag{1.8}$$

Each nucleus is characterized by a definite atomic number, Z, and mass number, A; for clarity, we use the symbol M to denote the atomic mass in kinematic equations. The atomic number Z is the number of protons, and hence the number of electrons, in the neutral atom; it reflects the atomic properties of the atom. The mass number A gives the number of nucleons: protons and neutrons; isotopes are nuclei (often called nuclides) with the same Z and different A. The current practice is to represent each nucleus by the chemical name with the mass number as a superscript (e.g., ^{12}C). For greater clarity, Z is sometimes written as a subscript, as in ${}_1^1\text{H}$, ${}_1^2\text{H}$, ${}_2^4\text{He}$, and so on.

The chemical atomic weight (or atomic mass) of elements as listed in the periodic table gives the average mass (i.e., the average of the stable isotopes weighted by their abundance). Carbon, for example, has an atomic weight of 12.011, which reflects the 1.1% abundance of ^{13}C.

The masses of particles may be expressed as given in Table 1.1 in terms of energy through the Einstein relation

$$E = Mc^2 \tag{1.9}$$

which associates 1 J of energy with $1/c^2$ of mass, where c is the velocity of light, $c = 2.998 \times 10^8$ m/s. The mass of an electron, m_e, is 9.11×10^{-31} kg, which is equivalent to an energy of

$$E = (9.11\times10^{-31}\,\text{kg})(2.998\times10^{8}\,\text{m/s})^2 = 8.188\times10^{-14}\,\text{J} = 0.511\,\text{MeV} \tag{1.10}$$

The Einstein relation also is useful when calculating the velocity, v, of an ion of mass M and energy E for a nonrelativistic energy domain where ion beam analysis energies are

$$v = \left(\frac{2E}{M}\right)^{1/2} = c\left(\frac{2E}{Mc^2}\right)^{1/2} \tag{1.11}$$

TABLE 1.1 Mass Energies of Particles and Light Nuclei

Particle	Symbol	Atomic Mass [u]	Mass [10^{-27} kg]	Mass Energy [MeV]
Electron	e or e^-	0.000549	9.1095×10^{-4}	0.511
Proton	p or $^1H^+$	1.007276	1.6726	938.3
Atomic mass unit (amu)	u	1.00000	1.6606	931.7
Neutron	n	1.008665	1.6747	939.6
Deuteron	d or $^2H^+$	2.01410	3.3429	1875.6
Alpha	α or $^4He^{2+}$	4.00260	6.6435	3727.4

For example, the velocity of a 2 MeV ^{4}He ion is

$$v = 3\times10^8 \text{ m/s}\left(\frac{2\times2\times10^6\ (\text{eV})}{3727\times10^6\ (\text{eV})}\right)^{1/2} = 9.8\times10^6 \text{ m/s}$$

1.4 THE BOHR VELOCITY AND RADIUS

The Bohr atom provides useful relations for simple estimates of atomic parameters. The Bohr radius of the hydrogen atom is given by

$$a_0 = \frac{\hbar^2}{m_e e^2} = 0.5292\times10^{-8}\text{cm} = 0.05292 \text{ nm} \tag{1.12}$$

and the Bohr velocity of the electron in this orbit is

$$v_0 = \frac{\hbar}{m_e a_0} = \frac{e^2}{\hbar} = 2.188\times10^8 \text{cm/s} \tag{1.13}$$

where $\hbar = h/2\pi$ with Planck's constant $h = 4.136 \times 10^{-15}$ eV s. For comparison with the Bohr radius, the radius of a nucleus is given by the empirical formula

$$R = R_0 A^{1/3} \tag{1.14}$$

where A is the mass number and R_0 is a constant equal to 1.4×10^{-13} cm. The nuclear radius is about four orders of magnitude smaller than the Bohr radius.

PROBLEMS

1.1. Aluminum is a face-centered-cubic metal with lattice parameter $a = 4.05 \times 10^{-8}$ cm. Calculate the density of atoms/cm^2 on a {200} planar face using
   a. The planar spacing, Equation (1.5), and $d_{200} = 0.203$ nm
   b. The relation

$$N_s = \frac{\text{surface atoms/unit cell}}{\text{surface cell area}}$$

1.2. For the canonical value of 10^{15} atoms/cm^2 in a monolayer on a cubic crystal, estimate
   a. The bulk density
   b. The volume Ω_V occupied by an atom

1.3. Nickel is a face-centered-cubic metal with an atomic weight of 58.7 and mass density of 8.91 g/cm^3.
   a. What are the atomic density of nickel and the atomic volume, Ω_V?
   b. What is the lattice parameter, a_c?

1.4. Silicon has a diamond cubic lattice structure with an atomic density of 5×10^{22} atoms/cm^3 and an atomic weight of 28.09.
   a. What are silicon's mass density and average areal density?
   b. What are silicon's lattice parameter and atomic volume, Ω_V?

1.5. Calculate the energy in electron volts of a proton moving at the Bohr velocity. What is the velocity of a 35 keV As ion?

1.6. What is the value of the K-shell radius for silicon (Z = 14), germanium (Z = 32), and gold (Z = 79)?

1.7. Estimate the nucleus size of ^{1}H, ^{4}He, ^{12}C, and ^{79}Au.

SUGGESTED READING

Cullity, B. D. 1978. *Elements of x-ray diffraction.* Boston, MA: Addison–Wesley Publishing Company, Inc.

Feldman, L. C., and Mayer, J. W. 1986. *Fundamentals of surface and thin film analysis.* New York: North–Holland.

Krane, K. S. 1988. *Introductory nuclear physics.* New York: John Wiley & Sons.

Omar, M. A. 1975. *Elementary solid state physics: Principles and applications.* Boston, MA: Addison–Wesley Publishing Company.

Weidner, R. T., and Sells, R. L. 1980. *Elementary modern physics,* 3rd ed. Boston, MA: Allyn & Bacon.

Kinematics

2

2.1 KINEMATICS OF ELASTIC COLLISIONS

The energy transfers and kinematics in elastic collisions between two isolated particles can be solved fully by applying the principles of conservation of energy and momentum. We consider those collisions in which the kinetic energy is conserved to be *elastic.* An *inelastic* collision does not conserve kinetic energy; an example is the promotion of electrons to higher energy states in collisions where substantial K-shell overlap occurs. The energy lost in promoting the electrons is not available in the particle–atom kinematics after the collision. In this chapter we consider only elastic processes.

For an incident energetic particle of mass M_1, the values of the velocity and energy are v_0 and E_0 ($E_0 = 1/2\, M_1 v_0^2$), while the target atoms of mass M_2 are at rest. After the collision, the values of the velocities v_1 and v_2 and energies E_1 and E_2 of the projectile and target atoms, respectively, are determined by the scattering angle θ and recoil angle ϕ. The notation and geometry for the laboratory system of coordinates are given in Figure 2.1. Table 2.1 is a list of symbols used in kinematic expressions.

Conservation of kinetic energy and conservation of momentum parallel and perpendicular to the direction of incidence are expressed by the equations

$$E_0 = \frac{1}{2} M_1 v_0^2 = \frac{1}{2} M_1 v_1^2 + \frac{1}{2} M_2 v_2^2 \tag{2.1}$$

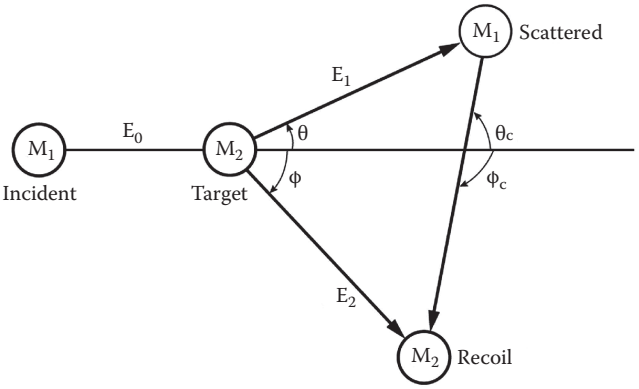

FIGURE 2.1 Elastic collision diagram between two unequal masses as seen in the laboratory reference frame with reference to CM reference frame scattering angles.

TABLE 2.1 Definitions and Symbols Used in Collision Kinematics

E_{-0}	Energy of the incident projectile
E_c	Total kinetic energy in the center-of-mass system
E_1	Laboratory energy of the scattered projectile
E_2	Laboratory energy of the recoiling target
T	Energy E_2 transferred to the target atom
θ_c	Center-of-mass variable scattering angle defined in Figure 2.1
K	Backscattering kinematic factor E_1/E_0
M_1	Mass of the incident projectile
M_2	Mass of the target particle
M_c	Reduced mass in center-of-mass system
X	Mass ratio M_1/M_2
v_0	Velocity of the incident projectile in laboratory coordinates
v_1	Velocity of the scattered projectile in laboratory coordinates
v_2	Velocity of the recoiling atom in laboratory coordinates
v_c	Velocity of the reduced mass in center-of-mass coordinates
v_{ion}	Velocity of the incident projectile (ion) in center-of-mass coordinates
v_{atom}	Velocity of the target atom in center-of-mass coordinates
θ	Laboratory angle of the scattered projectile
θ_c	Center-of-mass angle of the scattered projectile
θ_m	Maximum laboratory angle for M_1 scattering ($M_1 > M_2$)
ϕ	Laboratory angle of the recoiling target atom
ϕ_c	Center-of-mass angle of the recoiling target atom
π	$\pi = 180° = \theta_c + \phi_c$

$$M_1 v_0 = M_1 v_1 \cos\theta + M_2 v_2 \cos\phi \tag{2.2}$$

$$0 = M_1 v_1 \sin\theta - M_2 v_2 \sin\phi \tag{2.3}$$

Equations (2.1)–(2.3) can be solved in various forms; for example, transposing the first term on the right to the left side in Equations (2.2) and (2.3), squaring and adding, will eliminate ϕ, giving

$$(M_2 v_2)^2 = (M_1 v_0)^2 + (M_1 v_1)^2 - 2M_1^2 v_0 v_1 \cos\theta \tag{2.4}$$

Substituting Equation (2.4) into Equation (2.1) to eliminate v_2, one finds the ratio of the particle's velocity after and before the collision:

$$\frac{v_1}{v_0} = \frac{M_1}{M_1 + M_2}\cos\theta \pm \left[\left(\frac{M_1}{M_1 + M_2}\right)^2 \cos^2\theta + \frac{M_2 - M_1}{M_1 + M_2}\right]^{1/2} \tag{2.5}$$

Equation (2.5) can be used with Equation (2.4) to determine v_2 and E_2, and it can be used with Equation (2.2) to find the angle of recoil, ϕ, of the scattered target atom.

If $M_1 > M_2$, the quantity under the radical in Equation (2.5) will be zero for $\theta = \theta_m$, where θ_m is found from

$$\cos^2\theta_m = 1 - \frac{M_2^2}{M_1^2}, \qquad 0 \le \theta_m \le \frac{\pi}{2} \tag{2.6}$$

For $\theta > \theta_m$ (and θ), v_1/v_0 is either imaginary or negative, neither of which is physical, so θ_m represents the maximum angle through which M_1 can be scattered.

For the condition $M_1 < M_2$, all values of θ from 0 to π are possible, and a positive value for v_1/v_0 results if the plus sign in Equation (2.5) is chosen. Choice of the minus sign in this equation leads to negative values of v_1/v_0, which is physically unrealistic. The ratio of the projectile energies for $M_1 \le M_2$, where the plus sign holds, is

$$\frac{E_1}{E_0} = \left[\frac{\left(M_2^2 - M_1^2 \sin^2\theta\right)^{1/2} + M_1 \cos\theta}{M_2 + M_1}\right]^2 \tag{2.7}$$

This allows us to define the *kinematic factor* K,

$$K \equiv E_1/E_0 \tag{2.8}$$

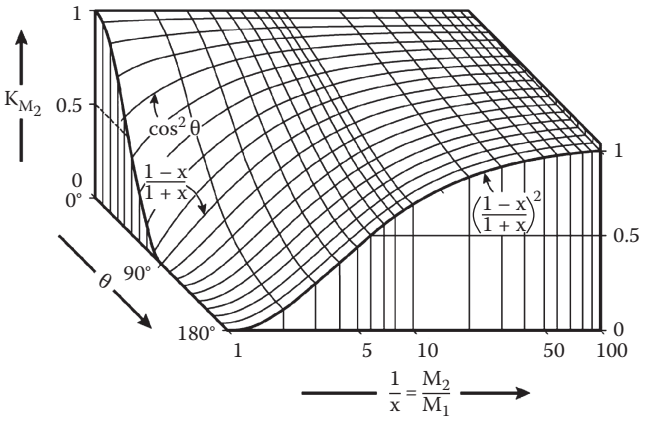

FIGURE 2.2 The kinematic factor K plotted as a function of scattering angle θ and mass ration $x^{-1} = M_2/M_1$. (Adapted from Chu, W.-K., Mayer, J. W., and Nicolet, M -A. 1978. *Backscattering spectrometry,* NY: Academic Press.)

Equation (2.7) can be rewritten as

$$K_{M_2} = \left[\frac{[1-(M_1/M_2)^2 \sin^2\theta]^{1/2} + M_1/M_2 \cos\theta}{1 + (M_1/M_2)}\right]^2 \tag{2.9}$$

where the subscript has been added to K to indicate the target mass for which the factor applies. Equation (2.9) shows that the kinematic factor depends only on the ratio of the projectile to the target masses and the scattering angle θ.

Figure 2.2 plots Equation (2.9) with the mass ratio $M_1/M_2 = x$. The plot of K versus $M_2/M_1 = x^{-1}$ and θ shows that for any combinations of projectile and target mass, K always has its lowest values at 180°. In addition, the value of K at $\theta = 180°$ is the square of its value at $\theta = 90°$. Also, for the condition of $M_1 = M_2$ (i.e., $x = 1$), the value of K is zero for $\theta > 90°$. The implication is that a projectile colliding with a target equal to its own weight cannot be scattered backward but only forward. This is also true for the condition $M_1 > M_2$.

The kinematic factor, as expressed by Equations (2.7)–(2.9), is the term in the applications of backscattering spectrometry for sensing the mass of target atoms. In backscattering spectrometry experiments the energy E_0 and mass M_1 of the projectile are known and the energy of the backscattered projectile E_1 is measured at angle θ. The only unknown is the mass of the target atom M_2 that prompted the backscattering event.

When a target contains two different atoms with mass difference ΔM_2 it is important that small differences in masses produce as large a change in ΔE_1 as possible if these masses are to be observed separately. Figure 2.2 shows that for fixed M_1 a change in ΔM_2 produces the largest change in K for $\theta = 180°$ for all but the smallest values of M_2.

In quantitative terms, for the condition that $\theta \sim 180°$, ΔM_2 and ΔE_1 are related to each other by (Chu, Mayer, and Nicolet 1978)

$$\Delta E_1 = E_0 \frac{1-x}{(1-x)^3} \left[4(1-x\delta^2) - \delta^2(1-x^2)\right] x \frac{\Delta M_2}{M_2} \tag{2.10}$$

where $\delta = \pi - \theta$. For $M_2 >> M_1$, this reduces to

$$\Delta E_1 = E_0 \left[4(1-x\delta^2)\left(M_1/M_2^2\right)\right] \Delta M_2 \tag{2.11}$$

Both Equations (2.10) and (2.11) show that ΔE_1 increases with E_0 and ΔM_2. This is demonstrated in Figure 2.3, where the backscattered ($\theta \sim 180$) energies for an He projectile (E_1) on targets of C, O, Si, Ti, and Bi for E_0 equal to 2 and 5 MeV are plotted separately. The normalized heights of these elements are indicative of their scattering strength or—more precisely, scattering cross section—that is discussed in Chapter 3.

Alternately, increases in ΔE_1 can also be accomplished by increasing M_1 (using a heavier incident ion beam such as Li). Keep in mind that M_2 values less than M_1 can produce forward scattering but will not produce any backscattering.

Additional equations related to Figure 2.1 are listed in Table 2.2.

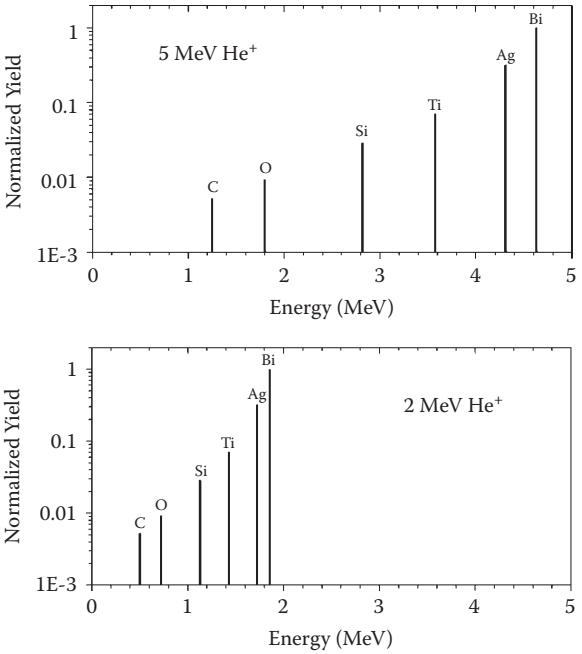

FIGURE 2.3 Energies for a He projectile (E_1) on targets of C, O, Si, Ti, and Bi for E_0 equal to 2 and 5 MeV in backscattering geometry ($\theta \sim 180$).

TABLE 2.2 Relationships between Energy and Scattering Angles

Center-of-mass energy	$E_c = \frac{M_2 E_0}{M_1 + M_2} = \frac{E_0}{1+x,}; \quad x = \frac{M_1}{M_2}$
Laboratory energy of the scattered projectile for $M_1 \le M_2$	$K = \frac{E_1}{E_0} = \frac{\left[x \cdot \cos\theta + \left(1 - x^2 \sin^2\theta\right)^{1/2}\right]^2}{(1+x)^2}$ When $M_1 = M_2, \theta \le \frac{\pi}{2}$
Laboratory energies of the scattered projectile for $M_1 > M_2$	$\frac{E_1}{E_0} = \frac{\left[x \cdot \cos\theta \pm (1 - x^2 \sin^2\theta)^{1/2}\right]^2}{(1+x)^2}$ $\theta \le \sin^{-1}(1/x)$
Laboratory energy of the recoil nucleus	$\frac{E_2}{E_0} = 1 - \frac{E_1}{E_0} = \frac{4M_1M_2}{\left(M_1 + M_2\right)^2} \cos^2\varphi =$ $\frac{4x}{(1+x)^2} \cos^2\varphi = \frac{4x}{(1+x)^2} \sin^2\left(\frac{\theta_c}{2}\right)$ where $\phi \le \frac{\pi}{2}$
Laboratory angle of the recoil nucleus	$\phi = \frac{\pi - \theta_c}{2} = \frac{\phi_c}{2} \qquad \sin\varphi = \left(\frac{M_1 E_1}{M_2 E_2}\right)^{1/2} \sin\theta$
Laboratory angle of the scattered projectile	$\tan\theta = \frac{M_2 \sin\theta_c}{M_1 + M_2 \cos\theta_c}$
Center-of-mass angle of the scattered projectile	$\theta_c = \pi - 2\phi = \pi - \phi_c$ When $M_1 \le M_2 \Rightarrow x \le 1, \theta_c$ is defined for all $\theta \le \pi$ and $\theta_c = \theta + \sin^{-1}(x \sin(\theta))$. When $M_1 > M_2 \Rightarrow x > 1, \theta_c$ is double valued and the laboratory scattering angle is limited to the range $\theta \le \sin^{-1}(1/x)$. In this case: $\theta_c = \theta + \sin^{-1}(x \sin\theta)$ or $\theta_c = \pi + \theta - \sin^{-1}(x \sin\theta)$

Source: Weller, R. 2009. Appendix 4 in *Handbook of Modern Ion Beam Materials Analysis*, 2nd ed., ed. Y. Wang and M. Nastasi, Warrendale, PA: MRS Publisher.

2.2 CLASSICAL TWO-PARTICLE SCATTERING

The collision and scattering problem defined by Figure 2.1 will now be restated in terms of center-of-mass (CM) coordinates. The motivation for this transformation will be obvious when we discuss scattering in a central force field later in this chapter. Through the use of CM coordinates it will be shown that no matter how complex the force is between the two particles, so long as it acts only along the line joining them (no transverse forces), the relative motion of the two particles can be reduced to that of a single particle moving in an interatomic potential centered at the origin of the center-of-mass coordinates. By introducing the CM system, the mutual interaction of the two colliding particles can be described by a force field, V(r), which depends only on the absolute value of the interatomic separation, r. The motion of both particles is given by one equation of motion. This equation has r as the independent variable and describes a particle moving in the central force field V(r).

The CM coordinates for a two-particle system are defined in a zero-momentum reference frame. In the frame, the total force on two particles that interact only with each other is zero. We can define the total force of two interacting particles as

$$\mathbf{F_T} = \mathbf{F_1} + \mathbf{F_2} = \frac{\mathbf{dp_T}}{\mathbf{d}t} \tag{2.12}$$

where $\mathbf{F_T}$ = total force, $\mathbf{F_1}$ and $\mathbf{F_2}$ are the individual forces on particles 1 and 2, respectively, and $\mathbf{p_T}$ is the total linear momentum of the two-particle system. For $\mathbf{F_T} = 0$, $d\mathbf{p_T} = 0$, indicating that the total momentum is unchanged or conserved during the interaction process.

One of the consequences associated with observing elastic collisions in the CM coordinates is that the individual particles' kinetic energies are unchanged by the collision process. Thus, the CM velocities of the two colliding particles are the same before and after the collision process. In addition, the CM scattering angle of particle 1 will equal the scattering angle of particle 2. Finally, all scattering angles in the CM system are allowed, unlike the scattering angles in the laboratory reference frame, where the allowed scattering angles depend on the ratio $x = M_1/M_2$.

The collision processes described in Figure 2.1 is represented in Figure 2.4. For CM coordinates, Figure 2.4(b), we define the system velocity, v_c, such that in this coordinate system there is no net momentum change, so

$$M_1 v_{\mathbf{0}} = \left(M_1 + M_2\right) v_{\mathbf{c}} \tag{2.13}$$

We also define in CM coordinates a reduced mass, M_c, given by the relation

$$\frac{1}{M_c} = \frac{1}{M_1} + \frac{1}{M_2} \tag{2.14}$$

or

$$M_c = \frac{M_1 M_2}{M_1 + M_2} \tag{2.15}$$

From Equations (2.13) and (2.15) we can represent the CM velocity in terms of reduced mass as

$$v_c = v_0 \frac{M_c}{M_2} \tag{2.16}$$

From the velocity vector diagram in Figure 2.4 and Equation (2.16), the ion and target atom velocities in CM coordinates are

$$v_{ion} = v_0 - v_c = v_0 \frac{M_c}{M_1} \tag{2.17}$$

$$v_{atom} = v_c = v_0 \frac{M_c}{M_2} \tag{2.18}$$

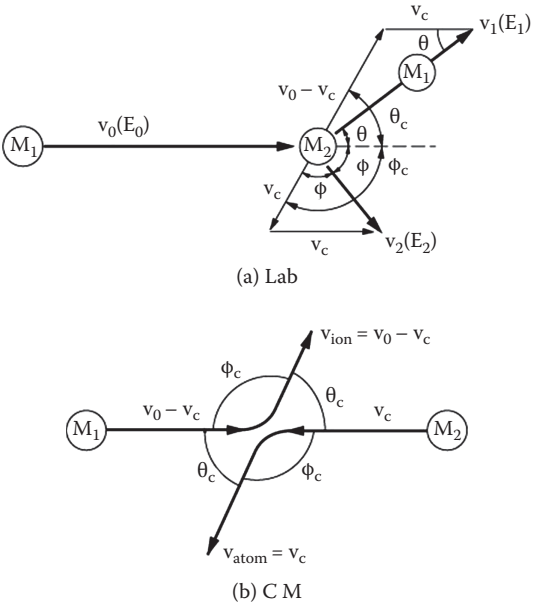

FIGURE 2.4 Schematic representation of classical two-particle scattering in (a) laboratory reference frame and (b) CM reference frame.

Equation (2.18) shows that the target atom, which has zero velocity before the collision in the laboratory reference frame, has the system velocity v_c before and after the collision in the CM reference frame.

Equations (2.17) and (2.18) show the advantage of the CM reference frame. The system velocity, v_c, and the atom and ion velocities, v_{atom} and v_{ion}, remain constant and are independent of the final scattering angle between the two particles (Figure 2.4b). Thus, regardless of whether the collision is elastic or inelastic, the total momentum is unchanged in a collision. In addition, from Equations (2.17) and (2.18), we see that the ratio of the ion to atom velocities is inversely proportional to the ratio of their masses:

$$\frac{v_{ion}}{v_{atom}} = \frac{v_0 - v_c}{v_c} = \frac{M_2}{M_1} = \frac{1}{x} \tag{2.19}$$

Another advantage to the CM reference frame is that the CM total energy, E_c, is equal to the CM initial kinetic energy:

$$E_c = \frac{1}{2} M_c v_0^2 \tag{2.20a}$$

$$E_c = \frac{1}{2} \frac{M_1 M_2}{M_1 + M_2} v_0^2 = \frac{M_2}{M_1 + M_2} E_0 \tag{2.20b}$$

where

$$E_0 = \frac{1}{2} M_1 v_0^2.$$

The conversion of scattering angles from the laboratory system to the CM system is determined from the scattering diagrams given in Figures 2.1 and 2.4. Examining the target atom (M_2) trajectory portion of Figure 2.4(a), we see that the final target velocity in the laboratory, v_2, is related to the CM atom velocity, $v_{atom} = v_c$, by the difference vector, v_c. Since the triangle formed by these velocity vectors is isosceles, we have

$$\phi_c = 2\phi \tag{2.21}$$

From the CM diagram, Figure 2.4(b), we have $\theta_c + \phi_c = \pi$, which allows us to rewrite Equation (2.21) in the form

$$\phi = \frac{\pi - \theta_c}{2} \tag{2.22}$$

which relates the target atom scattering angle in the laboratory to the CM ion scattering angle.

Another important relationship is the energy transferred to the target atom as a function of the target atom scattering angle θ_c or θ. Again, from the velocity vector diagram in Figure 2.4(a), and the law of cosines, we have

$$v_2^2 = v_c^2 + \left[v_c^2 - 2v_c^2 \cos(\pi - \phi_c) \right] \tag{2.23}$$

Using Equations (2.21) and (2.22) to recast ϕ_c in terms of θ_c, we obtain

$$v_2^2 = 2v_c^2 (1 - \cos \theta_c) \tag{2.24}$$

which relates the target atom recoil velocity in the laboratory to the CM velocity and the CM ion scattering angle. Equation (2.24) can be simplified by using Equations (2.18) and (2.21) to obtain

$$v_2 = 2v_0 \frac{M_c}{M_2} \cos \phi \tag{2.25}$$

which gives the laboratory recoil velocity, v_2, as a function of the initial ion velocity, v_0, and the laboratory recoil angle. This equation can now be used to obtain the energy transferred to the target atom by the incident ion through the kinetic energy velocity relationship,

$$E_2 = \frac{1}{2} M_2 v_2^2 \tag{2.26}$$

In many books, the energy *transferred* to the target atom, E_2, is referred to as T. Substituting Equation (2.25) into Equation (2.26) gives

$$T \equiv E_2 = \frac{M_2}{2} \left(\frac{v_0 M_c \cos\phi}{M_2} \right)^2 \tag{2.27}$$

The transferred energy, T, can be related to the ion scattering angle, θ_c, by Equation (2.22) to yield

$$T = \frac{2}{M_2} \left(v_0 M_c \sin \frac{\theta_c}{2} \right)^2 = \frac{4E_c M_c}{M_1} \sin^2 \frac{\theta_c}{2} \tag{2.28}$$

From the description of reduced mass, Equation (2.15), we rewrite Equation (2.28) to obtain

$$T = E_0 \frac{4M_1 M_2}{(M_1 + M_2)^2} \sin^2 \frac{\theta_c}{2} = T_M \sin^2 \frac{\theta_c}{2} \tag{2.29}$$

where T_m is the maximum energy transferable in a head-on collision when $\theta_c = 0$.

As an example, to determine the energy transferred in a binary collision where a 1 MeV boron ($M_1 = 10$) ion incident on Si ($M_2 = 28$) is scattered through a laboratory angle $\theta = 45°$, one first determines the corresponding CM angle θ_c from the

expression given in Table 2.1, $\theta_c = \theta + \sin^{-1}(x \sin\theta)$, which gives $\theta_c = 60°$. Next we calculate the ratio T_M/E from Equation (2.29), which gives $T_M = 0.78E_0$. Finally, for $E_0 = 1$ MeV, $T = 0.195$ MeV.

Additional relationships between the CM and the laboratory reference frames are summarized in Table 2.2.

2.3 THE CLASSICAL SCATTERING INTEGRAL

In this section we will derive an expression for the CM scattering angle θ_c. We will see that θ_c will depend on the interatomic potential V(r), the ion energy E, and the impact parameter, b.

We begin by defining the scattering trajectory of a moving particle in a central force field, assuming that the force between the two particles acts only along the line joining them and that there are no transverse forces. The use of CM coordinates then reduces any two-body problem to a one-body problem—namely, the interaction of a particle with mass M_c and velocity v_c with a static potential field, V(r), centered at the origin of the CM coordinates. This simplification occurs because in the CM system the *total linear momentum of the particles is always zero,* the paths of the two particles are symmetric (as shown in Figure 2.4), and the evaluation of the path of one particle (scattering angle) directly gives the path of the other particle. The conversion from CM scattering angles to laboratory angles is then achieved with the equations summarized in Table 2.2.

In Figure 2.5 we represent the scattering process between an atom moving with initial velocity v_0 and energy E_0 and a stationary target atom with the details of the scattering trajectories displayed for both the laboratory and the CM reference frames. The distance b in the figure is the *impact parameter* and defines the perpendicular distance between the initial position of the target atom and the incident trajectory of the ion. This parameter will be shown to be an important quantity in the scattering process and will define the hardness of the collision. The dashed lines in Figure 2.5 represent the asymptotes of the ion and target atom trajectories. The parameter r_{min} is the distance of closest approach during the scattering event.

Since we are dealing with two particles only and no transverse forces, the problem is two dimensional in the plane defined by the initial velocity vector for the ion and the initial position of the target atom. Since we are dealing with conservative central forces defined by an ion–atom interaction potential V(r), conservation of energy in the center-of-mass system will be

$$E_c = \frac{1}{2} M_c \left(\dot{\mathbf{r}}^2 + \mathbf{r}^2 \dot{\Theta}_c^2 \right) + V(r) \tag{2.30}$$

where the first term is the system kinetic energy. The variable r is defined in Figure 2.5 as

$$r = r_1 + r_2 \tag{2.31}$$

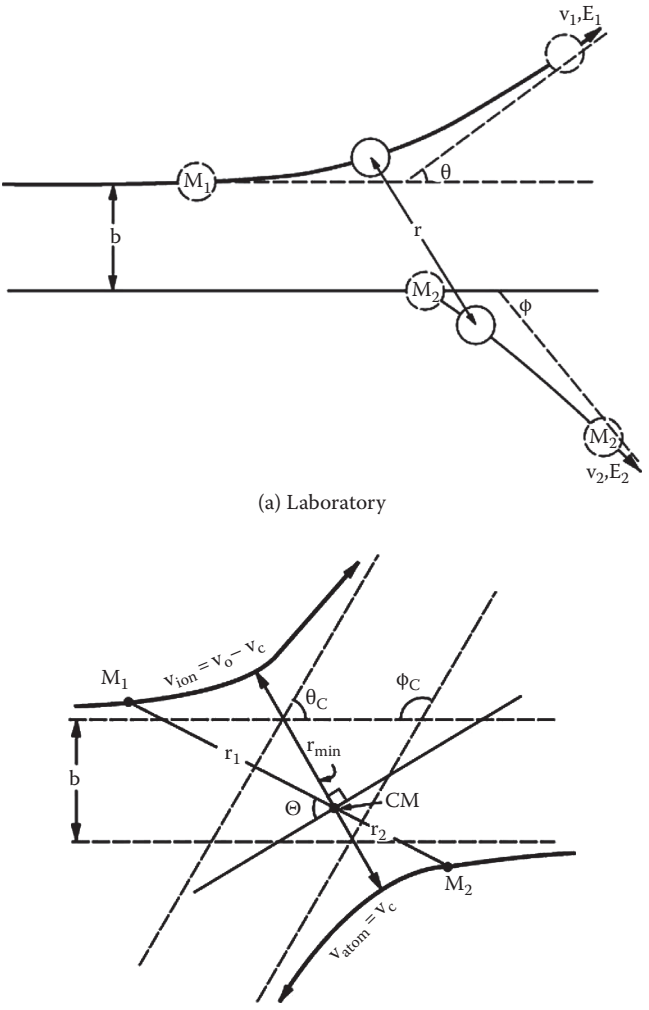

FIGURE 2.5 The collision trajectories at an impact parameter, b, for an elastic collision between two unequal masses, as seen in the (a) laboratory reference frame and (b) CM reference frame.

with the CM distances r_1 and r_2 defined by

$$r_1 = \frac{M_2}{M_1 + M_2} \quad r \tag{2.32a}$$

$$r_2 = \frac{M_1}{M_1 + M_2} \quad r \tag{2.32b}$$

The variable r is the CM separation distance between M_1 and M_2, and r_1 and r_2 represent the distance from the center of mass to the ion (M_1) and the target atom (M_2), respectively. The value $\dot{\Theta}_c$ is the time rate of change in the scattering angle, $d\Theta_c/dt$, and Θ_c is defined as the angle between line $r_1 + r_2$ and the line perpendicular to r_{min} and is different from the CM scattering angle θ_c. The energy E_c is the CM defined in Equation (2.20), and M_c is the CM defined in Equation (2.15).

In addition to the conservation of energy, we have the law of conservation of angular momentum that, during the scattering process in the CM system, is given by

$$\ell = M_c\, r^2\, \dot{\Theta}_c \tag{2.33}$$

where ℓ is the constant angular momentum. For large values of r, the angular momentum is simply related to the impact parameter and has the magnitude $M_c\, v_0\, b$. Since angular momentum is conserved, we have

$$\ell = M_c\, r^2\, \dot{\Theta}_c = M_c\, v_0\, b \tag{2.34}$$

from which we obtain

$$\dot{\Theta}_c = \frac{v_0 b}{r^2} \tag{2.35}$$

With Equations (2.20a), (2.30), and (2.35), we can now solve for Θ_c as a function of any central force potential, V(r). From these equations we obtain the radial equation of motion,

$$\dot{r} = v_0 \left(1 - \frac{V(r)}{E_c} - \left(\frac{b}{r}\right)^2\right)^{1/2} \tag{2.36}$$

Using Equations (2.35) and (2.36), and noting that $\dot{r} = dr/dt$ and that $\dot{\Theta}_c = d\Theta_c/dt$, we obtain

$$\frac{d\Theta_c}{dr} = \frac{d\Theta_c}{dt}\,\frac{dt}{dr} = \frac{b}{r^2\left[1 - \frac{V(r)}{E_c} - \left(\frac{b}{r}\right)^2\right]^{1/2}}. \tag{2.37}$$

The CM scattering angle θ_c is found by integrating Θ_c on the left-hand side of Equation (2.37) over the first half of the orbit, from $\theta_c/2$ to $\pi/2$,

which corresponds to the integration limits on the right-hand side of r_{min} to infinity:

$$\int_{\theta_c/2}^{\pi/2} d\Theta_c = \int_{r_{min}}^{\infty} \frac{b\, dr}{r^2\left[1 - \frac{V(r)}{E_c} - \left(\frac{b}{r}\right)^2\right]^{1/2}} \tag{2.38}$$

$$\frac{1}{2}(\pi - \theta_c) = \int_{r_{min}}^{\infty} \frac{b\, dr}{r^2\left[1 - \frac{V(r)}{E_c} - \left(\frac{b}{r}\right)^2\right]^{1/2}} \tag{2.39}$$

This reduces to

$$\theta_c = \pi - 2b\int_{r_{min}}^{\infty} \frac{dr}{r^2\left[1 - \frac{V(r)}{E_c} - \left(\frac{b}{r}\right)^2\right]^{1/2}} \tag{2.40}$$

This final equation is called the *classical scattering integral* and gives the angular trajectory information for two-body central-force scattering. Equation (2.40) allows us to evaluate the scattering angle θ_c in terms of energy, E_c; the interatomic potential, V(r); and the impact parameter, b. The scattering angle of an ion with energy E, moving in a force field defined by V(r), will vary with the impact parameter b. The significance of this will become clear when we discuss the differential scattering cross section in Chapter 3, where Equation (2.40) is solved explicitly for a Coulomb potential (Rutherford scattering). In general, potentials are more complex and numerical solutions are required. Transformations from the CM angle θ_c to the laboratory angles θ and ϕ can be made with the help of Table 2.2.

PROBLEMS

2.1. a. What is the velocity for a 1 MeV He ion and for a 1 MeV proton?
b. What is the velocity of a 1 MeV He ion after a 180° backscattering collision with a silicon atom?

2.2. What is the laboratory energy for 1 MeV He ions scattered from carbon at a scattering angle of 150°? How about if the He ions are replaced with the same energy of protons or lithium ions?

2.3. For a detector that can resolve a 30 keV energy difference, what change in mass can be detected by 2 MeV He ion scattering at 180°? Can you resolve two isotopes of Li and Cu with this system?

2.4. Suppose 1 MeV He ions interact with silicon atoms in an experiment:
   a. What is the reduced mass in the collision?
   b. Determine the final silicon atom velocity if the collision takes place at 90° (right angle).
   c. Find the center of mass angle for the silicon atom after a 90° (right angle) collision.

2.5. What is the maximum energy transferred in a head-on collision of a 1 MeV He ion with silicon? What are the corresponding energy and scattering angle of He ions after such a head-on collision?

2.6. Derive the expression for the laboratory energy of the recoil nucleus as written in Table 2.2.

2.7. Write a simple expression for E_1/E_0 and E_2/E_0 in backscattering (180°) and right angle scattering (90°) for $M_1 = M_2$, $M_1 > M_2$, and $M_1 < M_2$. What are the allowed solutions?

2.8. What is the maximum energy transferred to electrons, silicon atoms, and copper atoms by incident 1 MeV electrons, silicon ions, and copper ions?

2.9. In the laboratory system, we have He ions at 1 MeV scattered from silicon atoms at $\theta = 10°$:
   a. In the laboratory system what are v_1, v_2, ϕ, and E_2?
   b. In the center-of-mass system, what are v_{ion}, θ_c, and ϕ_c?

2.10. Solve the scattering integral, Equation (2.40) for the unscreened Coulomb potential $V(r) = Z_1Z_2e^2/4$.

REFERENCES

Weller, R. 2009. Appendix 4. In *Handbook of modern ion beam materials analysis*, 2nd ed., eds. Y. Wang and M. Nastasi. Warrendale, PA: MRS Publisher.

SUGGESTED READING

Chu, W.-K, Mayer, J. W., and Nicolet, M.-A. 1978. *Backscattering spectrometry,* chap. 2. New York: Academic Press.

Feldman, L. C., and Mayer, J. W. 1986. *Fundamentals of surface and thin film analyses.* New York: North–Holland Science Publishing.

French, A. P. 1971. *Newtonian mechanics.* New York: W. W. Norton and Co.

Goldstein, H. 1959. *Classical mechanics.* Reading, MA: Addison–Wesley Publishing Co.

Johnson, R. E. 1982. *Introduction to atomic and molecular collisions.* New York: Plenum Press.

Symon, K. R. 1953. *Mechanics.* Reading, MA: Addison–Wesley Publishing Co.

Torrens, I. M. 1972. *Interatomic potentials.* New York: Academic Press.
Weller, R. 1995. Appendix 4. In *Handbook of modern ion-beam materials analysis*, ed. J. R. Tesmer and M. Nastasi. Pittsburg: Materials Research Society.
Ziegler, J. F., Biersack, J. P., and Littmark, U. 1985. *The stopping and range of ions in solids.* New York: Pergamon Press Inc.

Cross Section

3

3.1 INTRODUCTION

In ion beam analysis experiments, many ions interact with many target nuclei. Due to the large number of interactions, the questions of how much energy will be transferred in a collision or what the scattering angle will be must be answered. The differential cross section is the fundamental parameter that we will develop. It gives a measure of either the probability of transferring energy T in the range between T and T + dT to a target atom or of the probability of scattering a projectile into some angle between θ_c and $\theta_c + d\theta_c$. We will discuss the scattering cross section in this chapter. Chapter 4 will deal with the stopping cross section that is related to the probability of energy transfer. The differential cross section has units of area, typically centimeters squared. The differential cross section integrated over all angles is the total cross section, often referred to simply as the cross section.

3.2 ANGULAR DIFFERENTIAL SCATTERING CROSS SECTION

It is customary to describe the number of particles scattered through different angles θ_c in terms of a quantity called the angular differential scattering cross section. Imagine the experiment depicted in Figure 3.1, where a beam of ions is incident on a thin foil and is scattered into a detector of area Δa at a polar angle between θ_c and $\theta_c + d\theta_c$. Each of the ions in the incident beam has a different impact parameter b (as described in Chapter 2) and will be scattered through a different angle. We

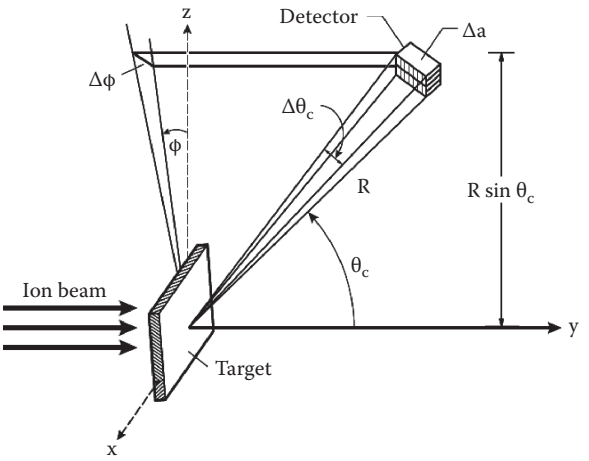

FIGURE 3.1 Experiment for measuring angular differential cross section. The detector area is $\Delta a = (R\Delta\theta_c)(R\sin\theta_c\Delta\varphi)$. By moving the detector to all angular positions for a fixed R, all the scattered particles can be counted, and the detector will have covered an area $4\pi R^2$, or a total solid angle of 4π.

define the differential dn_θ as the number of ions scattered into the detector of area Δa, between angles θ_c and $\theta_c + d\theta_c$, per unit time. We also define I_0 to be the flux of incident particles equal to the number of ions incident on the sample per unit time, per unit area (i.e., ions per second per centimeter squared). The solid angle of the detector, $\Delta\Omega$, is related to the detector area, Δa, and its distance away from the sample, R, and is given by

$$\Delta\Omega = \frac{\Delta a}{R^2} = \frac{(R\Delta\theta_c)(R\sin\theta_c\Delta\phi)}{R^2} = \Delta\theta_c\Delta\phi\ \sin\theta_c \tag{3.1}$$

We now define $d\sigma(\theta_c)$, the differential scattering cross section, to be given by

$$\frac{d\sigma(\theta_c)}{d\Omega} \equiv \frac{1}{I_0}\frac{dn_{\theta_c}}{d\Omega} \tag{3.2}$$

where, for $\Delta a \to 0$, we have $\Delta\Omega \to d\Omega$. The term $d\sigma(\theta_c)/d\Omega$ is the differential scattering cross section per unit solid angle, and $dn_{\theta_c}/d\Omega$ is the number of particles scattered into the angular regime between θ_c and $\theta_c + d\theta_c$ per unit solid angle, per unit time. Since the solid angle Ω units (steradian) are dimensionless, the differential scattering cross section has units of area.

The cross section is simply the effective target area presented by each scattering center (target nucleus) to the incident beam. At a more microscopic level, the scattering cross section can be shown to be dependent on b, the impact

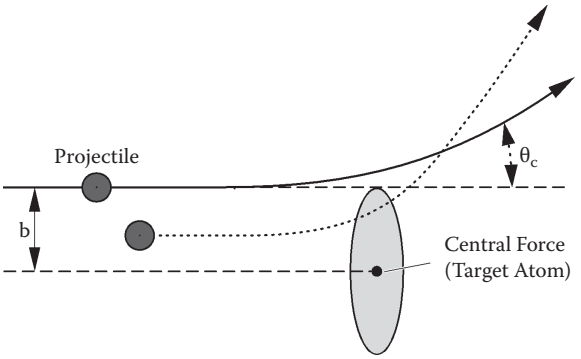

FIGURE 3.2 Scattering of a particle that approaches a nucleus with an impact parameter b. The total cross section is $\sigma = \pi b^2$.

parameter. In Figure 3.2 we present the collision process in which the incident particle is scattered by a target nucleus through an angle θ_c. The projectile moves in a nearly straight line until it gets fairly close to the target nucleus, at which point it is deflected through an angle θ_c. After being deflected, the trajectory of the particle is again nearly a straight line. If there had been no interaction force between the projectile and the target nucleus, the projectile would have maintained a straight trajectory and passed the target nucleus at a distance b.

Examining Figure 3.2, we see that all incident particles with impact parameter b are headed in a direction to strike the rim of the circle drawn around the target nucleus and will be deflected by an angle θ_c. The area of this circle is πb^2, and any particle with a trajectory that strikes anywhere within this area will be deflected by an angle greater than θ_c. The target area defined by the impact parameter is called the total cross section $\sigma(\theta_c)$:

$$\sigma(\theta_c) = \pi b^2 \tag{3.3}$$

For projectiles moving with small values of b, the cross section defined by Equation (3.3) will be small, but, due to the interaction forces, the scattering angle will be large. Thus, b is proportional to $\sigma(\theta_c)$, while I_0 and $\sigma(\theta_c)$ are inversely related to θ_c. From this discussion we see that $b = b(\theta_c)$.

In addition to the total cross section, there is the differential cross section, $d\sigma(\theta_c)$, and its relationship to b. As shown in Figure 3.3, particles incident with impact parameters between b and b + db will be scattered through angles between θ_c and $\theta_c + d\theta_c$. The differential cross section for this process is found by taking the differential of Equation (3.3) with respect to the impact parameter:

$$d\sigma(\theta_c) = d(\pi b^2) = 2\pi b\, db \tag{3.4}$$

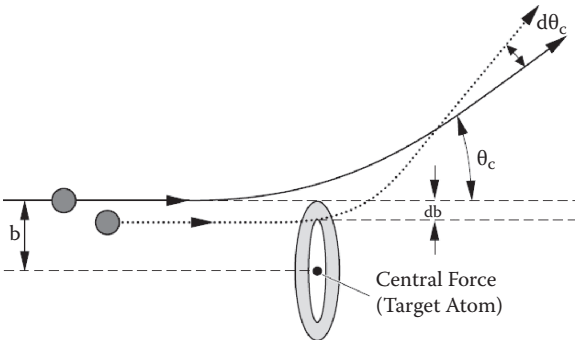

FIGURE 3.3 Nuclear target area for the differential cross section $d\sigma = 2\pi b db$.

From the description given in Equation (3.4) and the schematic presented in Figure 3.3, the differential cross section of each target nucleus is presented as a ring of radius b, a circumference $2\pi b$, and width db. Any incident particles with an impact parameter within db will be scattered into angles between θ_c and $\theta_c + d\theta_c$.

From the examples presented in Figures 3.2 and 3.3, we see that there is a unique connection between the value of I_0 and the scattering angle θ_c. To find the dependence of $d\sigma(\theta_c)$ on the scattering angle, we rewrite Equation (3.4) in the form

$$d\sigma(\theta_c) = 2\pi\ b(\theta_c)\left|\frac{db(\theta_c)}{d\theta_c}\right| d\theta_c \tag{3.5}$$

We use the absolute value of $db(\theta_c)/d\theta_c$ to maintain $d\sigma(\theta_c)$ as a positive value; θ_c increases as b decreases, indicating that $db(\theta_c)/d\theta_c$ is negative.

To determine an expression for the differential scattering cross section per unit solid angle (Equation 3.1), we note that scattering experiments are performed by observing the number of incident particles that are scattered into a solid angle located at θ_c. Measurements give information in units of the number of scattering particles per element of solid angle. A schematic of this process is presented in Figure 3.4. The annular region represents the solid angle $d\Omega$ subtended between the scattering angles θ_c and $\theta_c + d\theta_c$. The entire area of the sphere of radius R is $4\pi R^2$ and the total solid angle of the sphere is 4π. The shaded area is a ring of radius equal to R sin θ_c, circumference equal to $2\pi R \sin\theta_c$ and width of $Rd\theta_c$. The area of the shaded region is therefore $(2\pi)(R \sin\theta_c)(R\ d\theta_c) = 2\pi R^2 \sin\theta_c\ d\theta_c$. By definition of solid angle, area/R^2, we obtain

$$d\Omega = 2\pi\ \sin\ \theta_c d\theta_c \tag{3.6}$$

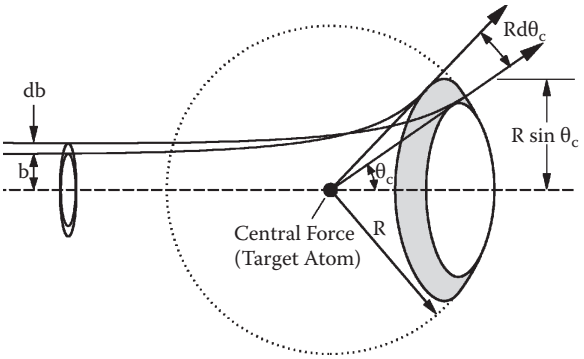

FIGURE 3.4 The solid angle dΩ subtended at the scattering angle θ_c by the incremental angle $d\theta_c$. By definition, $d\Omega/4\pi$ is the shaded area divided by the entire area of spherical surface; the shaded area is equal to $2\pi(R\sin\theta_c)(Rd\theta_c)$. Then, $d\Omega/4\pi = 2\pi R^2 \sin\theta_c d\theta_c)/4\pi^2$; therefore, $d\Omega = 2\pi \sin\theta_c d\theta_c$.

The result is equivalent to Equation (3.1), where $\Delta\phi$ has been integrated over 2π. The differential scattering cross section for scattering into a solid angle (Equation 3.1) is obtained by combining Equations (3.5) and (3.6) to produce

$$\frac{d\sigma(\theta_c)}{d\Omega} = \frac{b}{\sin\theta_c}\left|\frac{db}{d\theta_c}\right| \tag{3.7}$$

Equations (3.5) and (3.7) give the differential scattering cross section in the center of mass. The equivalent expressions in the laboratory reference frame can be obtained for the scattered projectile and scattered target nucleus by using the angular relationships presented in Table 2.2 in Chapter 2.

Integration of Equation (3.7) provides a relationship between the differential scattering cross section and the impact parameter:

$$\int_0^b b(\theta_c)\,db = \int_{\theta_c}^{\pi} \frac{d\sigma(\theta_c)}{d\Omega}\ \sin\theta_c\ \ d\theta_c$$

This results in the expression

$$b^2 = 2\int_{\theta_c}^{\pi} \frac{d\sigma(\theta_c)}{d\Omega}\ \sin\theta_c\ \ d\theta_c \tag{3.8}$$

where the dependence of scattering angles on the impact parameter has been omitted for brevity. By linking Equation (3.8) with the expression for θ_c (Equation 2.40 in Chapter 2), an effective means of passing between V(r) and $d\sigma(\theta_c)$ can be established.

3.3 RUTHERFORD DIFFERENTIAL CROSS SECTION

As an example of the use of the angular differential cross section, we consider the condition where the interaction between colliding particles is purely Coulombic, as is the case for Rutherford scattering; for this situation the projectile and target nucleus are treated as pure nuclei, with the projectile described by mass and atomic number M_1 and Z_1 and the target nucleus described by mass and atomic number M_2 and Z_2. The interatomic potential for Coulomb interaction in the centimeter–gram–second (cgs) unit is given by

$$V(r) = \frac{Z_1 Z_2 e^2}{r} \tag{3.9}$$

where r is the distance of separation between the two nuclei. To put Equation (3.9) into the same form as Equation (2.40), we make the following substitutions:

$$u \equiv \frac{1}{r} \tag{3.10a}$$

and

$$\alpha = Z_1 Z_2 e^2 \tag{3.10b}$$

leading to

$$V(u) = \alpha u \tag{3.11}$$

With the interatomic potential written in this way, the angular scattering integral (Equation 2.40) becomes

$$\theta_C = \pi - 2 \int_0^{1/r_{min}} \frac{du}{\left[\frac{1}{b^2} - \frac{\alpha u}{E_c b^2} - u^2\right]^{1/2}} \tag{3.12}$$

Equation (3.12) can be integrated exactly by noting the following integral solution:

$$\int \frac{dx}{(a + cx + dx^2)^{1/2}} = \frac{-1}{(-d)^{1/2}} \sin^{-1}\left(\frac{c + 2dx}{(q)^{1/2}}\right)$$

where $q = c^2 = 4ad$. For Equation (3.12) these variables are equal to

$$a = \frac{1}{b^2}; \quad c = \frac{-\alpha}{E_c\, b^2}; \quad d = -1$$

$$q = \frac{4}{b^2}\left(1 + \frac{\alpha^2}{4E_c^2\, b^2}\right)$$

and

$$c + 2dx = -\left(2u + \frac{\alpha}{E_c\, b^2}\right)$$

Carrying out these substitutions, the solution to Equation (3.12) is now given by

$$\theta_c = \pi - 2\left[\sin^{-1}\left(\frac{-\left(bu + \frac{\alpha}{2E_c b}\right)}{\left(1 + \frac{\alpha^2}{4E_c^2 b^2}\right)^{1/2}}\right)\right]_0^{1/r_{min}} \tag{3.13}$$

To complete the integration, a value for r_{min} must first be obtained. It can be shown from the law of conservation of angular momentum that the distance of closest approach, r_{min}, is related to the ion energy, E_c, and the form of the interatomic potential, $V(r_{min})$, through the following expression (Nastasi, Mayer, and Hirvonen 1996)

$$0 = 1 - \frac{V(r_{min})}{E_c} - \frac{b^2}{r_{min}^2}$$

Using the change in variables defined by Equations (3.10) and (3.11), we have

$$b^2 u_{min}^2 + \frac{\alpha u_{min}}{E_c} - 1 = 0 \tag{3.14}$$

where $u_{min} = 1/r_{min}$. Equation (3.14) is solved for μ_{min} using the quadratic equation, and it has the solution

$$u_{min} = \frac{1}{r_{min}} = \frac{1}{b}\left(\frac{-\alpha}{2bE_c} \pm \left(\left(\frac{\alpha}{2bE_c}\right)^2 + 1\right)^{1/2}\right). \tag{3.15}$$

Applying Equation (3.15) to the upper limit in Equation (3.13) gives

$$\theta_c = \pi - 2\left\{\pm\frac{\pi}{2} - \sin^{-1}\left(\frac{\frac{\alpha}{2E_c b}}{\left(1+\left(\frac{\alpha}{2E_c b}\right)^2\right)^{1/2}}\right)\right\} \tag{3.16}$$

This can be rewritten as

$$\frac{\theta_c - \pi}{2} = \pm\frac{\pi}{2} + \sin^{-1}\left(\frac{\alpha}{2E_c b}\left[1+\left(\frac{\alpha}{2E_c b}\right)^2\right]^{-1/2}\right) \tag{3.17}$$

We now use Equation (3.17) to express b in terms of θ_c. Equation (3.17) can be rewritten as

$$\sin\left(\frac{\theta_c - \pi}{2} \pm \frac{\pi}{2}\right) = \pm\sin\left(\frac{\theta_c}{2}\right) = \frac{\frac{\alpha}{2E_c b}}{\left[1+\left(\frac{\alpha}{2E_c b}\right)^2\right]^{1/2}}$$

The trigonometric representation of this equation is presented in Figure 3.5, which allows us to construct the following relationship between the impact parameter b and the scattering angle θ_c:

$$b = \frac{\alpha}{2E_c}\cot\left(\frac{\theta_c}{2}\right) = \frac{\alpha}{2E_c}\frac{\cos(\theta_c/2)}{\sin(\theta_c/2)}. \tag{3.18}$$

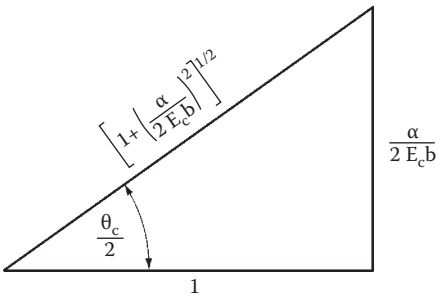

FIGURE 3.5 Trigonometric relation between the center of mass scattering angle, θ_c, and the impact parameter, b, for the Coulomb potential.

We will now use Equation (3.18) together with Equation (3.7), $d\sigma(\theta_c)/d\Omega = b/\sin\theta_c\,|db/d\theta_c|$, to obtain the differential cross section for scattering into a solid angle $d\Omega$ for the Coulomb potential. Differentiating Equation (3.18) with respect to θ_c,

$$\frac{db}{d\theta_c} = \frac{\alpha}{2E_c}\,\frac{d(\cot(\theta_c/2))}{d\theta_c} = \frac{\alpha}{2\,E_c}\,\frac{d}{d\theta_c}\left(\frac{\sin(\theta_c/2)}{1-\cos(\theta_c/2)}\right) = \frac{\alpha}{4E_c\sin^2(\theta_c/2)} \tag{3.19a}$$

and, multiplying by b,

$$b\frac{db}{d\theta_c} = \frac{1}{2}\left(\frac{\alpha}{2E_c}\right)^2\frac{\cot(\theta_c/2)}{\sin^2(\theta_c/2)} \tag{3.19b}$$

leads to

$$\frac{d\sigma(\theta_c)}{d\Omega} = \frac{b}{\sin\theta_c}\left|\frac{db}{d\theta_c}\right| = \frac{1}{2}\left(\frac{\alpha}{2E_c}\right)^2\frac{\cot(\theta_c/2)}{\sin\theta_c\ \sin^2(\theta_c/2)}$$

or

$$\frac{d\sigma(\theta_c)}{d\Omega} = \left(\frac{\alpha}{4\,E_c}\right)^2\frac{1}{\sin^4(\theta_c/2)} \tag{3.20}$$

where the geometrical relation $\sin\theta_c = 2\sin(\theta_c/2)\cos(\theta_c/2)$ has been used.

For 1 MeV ^{4}He ions ($Z_1 = 2$) incident on silicon ($Z_2 = 14$), the value of E_c = 875 keV and α = 40.3 eV nm. For a 180° backscattering event, $\theta_c/2 = 90°$ and $\sin^4(\theta_c/2) = 1$. Then, $d\sigma(\theta_c)/d\Omega = (\alpha/E_c)^2 = 1.3 \times 10^{-10}$ nm^2, or a value of 1.3×10^{-24} cm^2. For forward scattering at $\theta_c = 2°$, the expression $\sin^4(\theta_c/2) = 1\times10^7$, indicates a ratio of seven orders of magnitude between forward scattering at 2° and backscattering at 180°.

The angular differential cross section is obtained from the relationship between $d\Omega$ and $d\theta_c$ defined in Equations (3.6), $d\Omega = 2\pi\,\sin\,\theta_c\,d\theta_c$, and (3.20). Using some differential algebra we have

$$\frac{d\sigma(\theta_c)}{d\,\theta_c} = \frac{d\sigma(\theta_c)}{d\Omega}\,\frac{d\Omega}{d\theta_c} = 2\pi\left(\frac{\alpha}{2E_c}\right)^2\frac{\cos(\theta_c/2)}{\sin^3(\theta_c/2)} \tag{3.21}$$

Equations (3.20) and (3.21) are the Coulomb angular differential scattering cross sections, otherwise known as the *Rutherford differential cross section.* From Equations (3.20) and (3.21) we see from the $\sin(\theta_c/2)$ term in the denominator that both $d\sigma(\theta_c)/d\theta_c$ and $d\sigma(\theta_c)/d\Omega$ increase as θ_c decreases. This indicates that the Coulomb scattering process favors small-angle scattering or, in other words, that the largest cross sections are for scattering events of small angles.

For forward scattering at $\theta_c = 2°$, the expression $\sin^4(\theta_c/2) = 1\times10^7$, indicates a ratio of seven orders of magnitude between forward scattering at 2° and backscattering at 180°.

A complete analysis of the scattering problem and transforming Equation (3.20) to the laboratory frame of reference yields (Chu, Mayer, and Nicolet 1978)

$$\frac{d\sigma(\theta)}{d\Omega} = \left(\frac{Z_1 Z_2 e^2}{4E}\right)^2 \frac{4}{\sin^4\theta} \frac{\{[1-((M_1/M_2)\sin\theta)^2]^{1/2} + \cos\theta\}^2}{[1-((M_1/M_2)\sin\theta)^2]^{1/2}} \tag{3.22}$$

3.4 NON-RUTHERFORD CROSS SECTIONS

The derivation of the Rutherford cross section assumes that the interaction between the particle Z_1 and the target atom Z_2 is well described by the Coulomb potential V(r). For this assumption to be correct, the particle velocity must be sufficiently large so that the particle penetrates well inside the orbitals of the atomic electrons. Under such conditions, the scattering will be due to the repulsion of the two positively charged nuclei of atomic numbers Z_1 and Z_2. However, experimental measurements indicate that the actual cross sections depart from the Rutherford at both high and low energies. The low-energy departures are caused by partial screening of the nuclear charge by the electron shells surrounding both nuclei, and the high-energy departures are caused by the interaction of the nuclei and presence of short-range nuclear forces. Typically, the real cross section, σ, is expressed in terms of the Rutherford cross section, σ_R, as

$$\sigma = F\sigma_R \tag{3.23}$$

where F is a correction factor.

On the low-energy side we can estimate when electron screening effects become important. For the Coulomb potential to be valid, we require that a parameter called the distance of closest approach, d, be smaller than the K-shell electron radius. The distance of closest approach is given by

$$d = \frac{Z_1 Z_2 e^2}{E} \tag{3.24}$$

where e is the charge on the electron, e^2 has the value of 1.44 eV nm, and E is the particle energy. In this analysis the K-shell electron radius can be estimated as a_0/Z_2 where a_0 = 0.053 nm, the Bohr radius. Using Equation (3.24) and the requirement that d be less than the K-shell electron radius sets the lower limit of the energy of the analysis beam to be

$$E > Z_1 Z_2^2 \frac{e^2}{a_0} \tag{3.25}$$

This energy value corresponds to ~10 keV for He scattered from Si (Z_2 = 14) and 340 keV for He scattered from Au (Z_2 = 79). In practice, low-energy deviations from Rutherford occur at energies greater than the estimate given by Equation (3.25), as part of the particle trajectory is always outside the target atom's electron cloud. Results of several investigations indicate that the low-energy correction factor F in Equation (3.23) is given with adequate accuracy for light-ion analysis beams with MeV energies by

$$F \equiv \frac{\sigma}{\sigma_R} = 1 - \frac{0.049\, Z_1 Z_2^{4/3}}{E_{CM}} \tag{3.26}$$

where E_{CM} is the center of mass energy in kiloelectron volts. In practice, replacing E_{CM} by the laboratory energy produces negligible error. For 1 MeV He ions on Au atoms, the correction factor corresponds to only ~3%.

At higher energies, departures from Rutherford scattering are due to nuclear interaction. Recent measurements and calculations regarding the onset of these high-energy departures from Rutherford backscattering are shown in Figure 3.6 for ^{4}He ions as a function of center of mass energy and target atomic number Z_2 (Bozoian 2009). The straight line in Figure 3.6 represents a rough boundary separating the region of Rutherford behavior (below the line) from the region where the cross section deviates from Rutherford by 4% (above the line). The equation resulting from a least-squares fit to the points in Figure 3.6 is

$$\text{For } ^4\text{He: } E_{CM} \cong 0.249\, Z_2 - 0.080 \tag{3.27}$$

The laboratory energy for the transition to non-Rutherford scattering for oxygen atoms (Z_2 = 8) can be calculated using Equation (3.27), and the relationship between center-of-mass and laboratory energies is given in Table 2.2, $E_{CM} = M_2 E_0/(M_1 + M_2)$. This calculation shows that the transition to non-Rutherford scattering should occur at E_0 = 2.39 MeV. Figure 3.7 shows the experimentally measured correction factor σ/σ_R for alpha particle (i.e., ^{4}He) backscattering (θ = 165°) on oxygen (Z_2 = 8). These data show that the cross sections remain Rutherford (i.e., σ/σ_R = 1) up to ~2.4 MeV, with the deviation

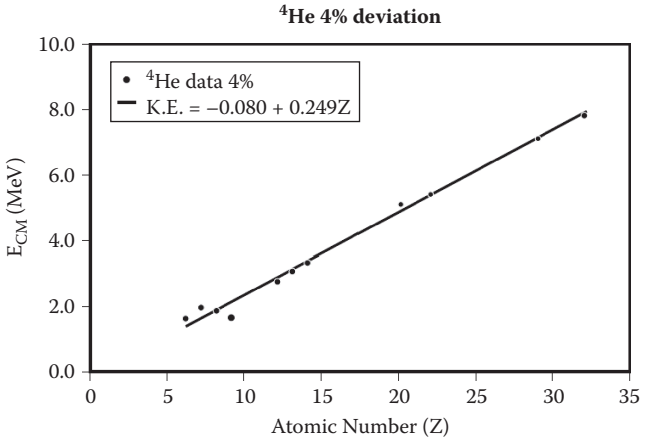

FIGURE 3.6 The center-of-mass ^{4}He ion energy at which the scattering cross section deviates by 4% from its Rutherford value as a function of atomic number.

from Rutherford first resulting in the corrections factor dropping below 1 and then increasing to values greater than 1. Also visible in Figure 3.7 is the strong increase (resonance) in the scattering cross section at ~3.045 MeV. The correction factor at this energy is ~15, or the cross section is 15 times the Rutherford. This enhancement in cross section can be used to increase the sensitivity to the detection of oxygen. Indeed, many nuclear scatterings and nuclear reactions are useful for light elemental detection, as will be described in Chapters 5 and 9.

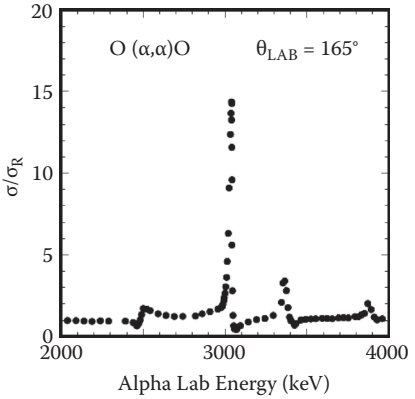

FIGURE 3.7 Experimentally measured normalized cross section for He scattering from oxygen.

PROBLEMS

3.1. A silicon surface barrier detector 2 cm in diameter is placed 4 cm away from the target. What is the solid angle of the detector?

3.2. (a) For 4 MeV He atoms incident on silicon, what is the impact parameter b? (b) Compare b to the actual size of the silicon nucleus. (c) What is the total scattering cross section?

3.3. What is the interatomic potential for a 1 MeV He ion incident at a distance of half the atomic spacing of a silicon lattice? Compare that to the value of b.

3.4. (a) What is the value of the closest approach, r_{min}, for 2 MeV He ions incident on silicon? (b) What is the value of the interatomic potential $V(r_{min})$?

3.5. For 1 MeV protons incident on germanium (Z = 32), what is the value of E_c and α?

3.6. Using Equation (3.22), calculate the differential scattering cross section per solid angle for 2 MeV He ions incident on Ni for laboratory scatterings of 10°, 15°, and 45°.

3.7. Transpose Equation (3.20) to the laboratory reference frame using equations in Table 2.2 in Chapter 2.

3.8. Show that, for the condition of $M_1 << M_2$, Equation (3.22) can be reduced to

$$\frac{d\sigma(\theta)}{d\Omega} = \left(\frac{Z_1 Z_2 e^2}{4E}\right)^2 \left[\sin - 4\frac{\theta}{2} - 2\left(\frac{M_1}{M_2}\right)^2 + \ldots\right]$$

Hint: expand in a power series.

3.9. A beam of 2 MeV He ions is incident on a silver foil and undergoes Coulomb scattering in accordance with the Rutherford formula:
   a. What is the distance of closest approach?
   b. What is the impact parameter for He ions scattered through 90°?
   c. If the silver specimen is mounted as a free-standing foil of 100 nm thickness, what is the fraction of number of the incident He ions being backscattered ($\theta \geq 90°$) by the foil?

3.10. A beam of He ions is incident on a gold foil:
   a. What is the Rutherford scattering cross section at $\theta = 170°$ if the He ion energy is 2 MeV?

b. At what He ion energy does the nuclear force become not negligible and the scattering cross section of this system start to deviate by 4% from the Rutherford?
c. At what He ion energy will the electron screening reduce the Rutherford cross section by 10% for this system?

3.11. Estimate the energy ranges for He ions incident on C, O, Si, Ti, Ag, and U where their scattering cross sections do not deviate more than 4% from the Rutherford values.

REFERENCES

Bozoian, M. 2009. *Handbook of modern ion beam analysis,* 2nd ed., eds. Y. Wang and M. Nastasi, Appendix 8. Warrendale, PA: Materials Research Society.

Chu, W.-K., Mayer, J. W., and Nicolet, M.-A. 1978. *Backscattering spectrometry,* chap. 2. New York: Academic Press.

Nastasi, M., Mayer, J. W., and Hirvonen, J. 1996. *Ion–solid interactions: Fundamentals and applications.* Cambridge: Cambridge University Press.

SUGGESTED READING

Alford, T. L., Feldman, L. C., and Mayer, J. W. 2007. *Fundamentals of nanoscale film analyses.* New York: Springer.

French, A. P. 1971. *Newtonian mechanics.* New York: W. W. Norton and Co.

Goldstein, H. 1959. *Classical mechanics* Reading, MA: Addison–Wesley Publishing Co.

Johnson, R. E. 1982. *Introduction to atomic and molecular collisions.* New York: Plenum Press.

Symon, K. R. 1953. *Mechanics.* Reading, MA: Addison–Wesley Publishing Co.

Weidner, R. T., and Sells, R. L. *Elementary modern physics,* 3rd ed. Boston: Allyn and Bacon Inc.

Ziegler, J. F., Biersack, J. P., and Ziegler, M. D. 2008. *The stopping and range of ions in matter.* Chester, MD: SRIM Co.

Ion Stopping

4

4.1 INTRODUCTION

When an energetic ion penetrates a solid, it undergoes a series of collisions with the atoms and electrons in the target. In these collisions the incident particle loses energy at a rate of dE/dx of a few to a hundred electron volts per nanometer, depending on the energy and mass of the ion as well as on the substrate material. It is these energy loss processes that allows depth information to be obtained in ion beam analysis.

The main parameters governing the energy-loss rate are the energy, E_0, and atomic number, Z_1, of the ion and atomic number, Z_2, of the substrate if we exclude the effect of the orientation of the crystal lattice. As the incident ion penetrates the solid undergoing collisions with atoms and electrons, the distance traveled between collisions and the amount of energy lost per collision are random processes. Hence, all ions of a given type and incident energy do not have the same distance traveled for the same energy loss; conversely, for the same distance traveled by an ion, there will be a spread in the energy lost. This distribution in energy loss is referred to as energy straggling.

4.2 THE ENERGY-LOSS PROCESS

The energy-loss rate dE/dx of an energetic ion moving through a solid is determined by ion interactions with the substrate atoms and electrons. It is customary to distinguish two different mechanisms of energy loss: (1) nuclear collisions, in which energy is transmitted

as translatory motion to a target atom as a whole; and (2) electronic collisions, in which the moving particle loses its kinetic energy by exciting or ejecting atomic electrons. For most purposes, this separation into elastic (nuclear) and inelastic (electronic) collisions is a convenient one and, although not strictly true, it is a good approximation. The energy-loss rate dE/dx can thus be expressed as

$$\frac{dE}{dx} = \left.\frac{dE}{dx}\right|_n + \left.\frac{dE}{dx}\right|_e \tag{4.1}$$

where the subscripts n and e denote nuclear and electronic collisions, respectively.

Nuclear collisions can involve large, discrete energy losses and significant angular deflection of the trajectory of the ion (Figure 4.1). This process is responsible for the production of lattice disorder by the displacement of atoms from their positions in the lattice as well as direct backcsattering events in Rutherford backscattering spectrometry. Electronic collisions involve much smaller energy losses per collision, negligible deflection of the ion trajectory, and negligible lattice disorder. The relative importance of the two energy-loss mechanisms changes rapidly with the velocity and atomic number Z_1 of the projectile: Nuclear stopping predominates for low velocity and high Z_1, whereas electronic stopping takes over for high velocity and low Z_1. A comparison of the nuclear and electronic energy loss rates expressed in reduced energy notation ε is shown in Figure 4.2. The reduced energy ε is expressed as

$$\varepsilon = \frac{E\, a_{TF}\, M_2}{Z_1 Z_2 e^2 (M_1 + M_2)} \tag{4.2}$$

where $e^2 = 1.44$ eV nm and a_{TF} is the Thomas–Fermi screening length, given by

$$a_{TF} = \frac{0.885\, a_0}{\left(Z_1^{1/2} + Z_2^{1/2}\right)^{2/3}} \tag{4.3}$$

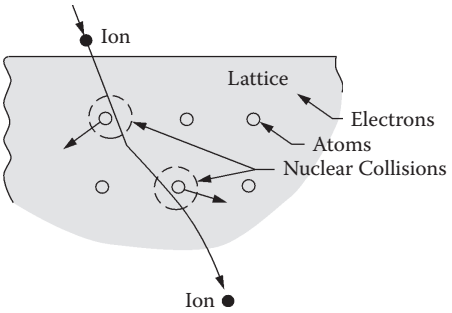

FIGURE 4.1 An ion incident on a crystal lattice is deflected in nuclear collisions with the lattice atoms and also loses energy in collisions with electrons. After passing through the sample it has lost DE in energy.

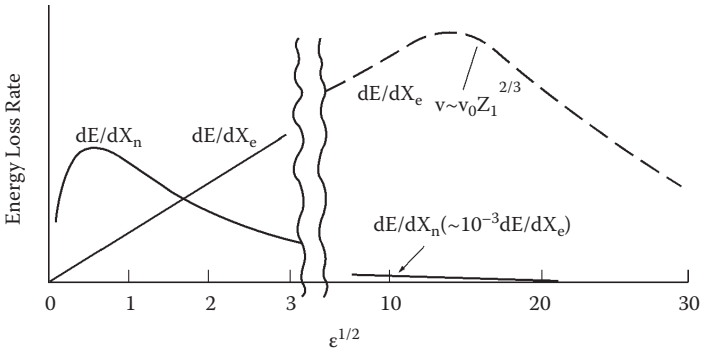

FIGURE 4.2 The reduced nuclear and electronic stopping as a function of $\varepsilon^{1/2}$.

With a_0, the Bohr radius is 0.053 nm. For the condition of 1 MeV He ions on a Si target, the Thomas–Fermi screening length $a_{TF} = 1.57 \times 10^{-2}$ nm and the corresponding reduced energy $\varepsilon = 341$.

Given that ε is proportional to ion energy E, the x axis of Figure 4.2, given in units of $\varepsilon^{1/2}$, is proportional to ion velocity. For 1 MeV He on Si, the value of $\varepsilon^{1/2}$ is ~18.5, which, according to Figure 4.2, is in the regime where the nuclear energy loss rate is approximately three orders of magnitude less than the electronic energy loss rate. This will be the case for most ion beam analysis conditions. As a result we will only treat high-energy electronic energy loss in this chapter. The reader is referred to other textbooks for treatments of low-energy electronic energy loss and nuclear energy loss (Nastasi, Mayer, and Hirvonen 1996; Ziegler, Biersack, and Ziegler 2008).

4.3 STOPPING CROSS SECTION

In addition to the energy-loss rate, it is also customary to speak of ε^A, the stopping cross section of element A, which is defined as

$$\varepsilon^A \equiv \frac{dE/dx}{N} \tag{4.4}$$

where N is the atomic density. The stopping cross section can be thought of as the energy-loss rate per scattering center. The stopping cross section has typical units of

$$\frac{dE/dx}{N}\left(\text{units: } \frac{(\text{eV/cm})}{(\text{atoms/cm}^3)} = \left(\frac{\text{eV cm}^2}{\text{atom}}\right)\right)$$

The nomenclature of stopping cross sections comes from the unit of area in the numerator.

4.4 ELECTRONIC STOPPING

As we discussed in Section 4.2, the energy-loss rate of ions in solids is divided into two different mechanisms of energy loss: the energy transferred by the ion to the target nuclei (called nuclear stopping) and the energy transferred by the ion to the target electrons (called electronic stopping). The relative importance of the various interaction processes between the ion and the target medium depends mostly on the ion velocity and on the charges of the ion and target atoms.

At ion velocities, v, significantly lower than the Bohr velocity of the atomic electrons v_0 (2.188×10^8 cm/s), the ion carries its electrons and tends to neutralize by electron capture. At these velocities, elastic collisions with the target nuclei, the nuclear energy loss, dominate. However, as the ion velocity is increased, the nuclear energy loss diminishes as $1/E_0$. The electronic energy loss (i.e., collisions with the atomic electrons) soon becomes the main interaction. The total energy loss is obtained as a sum of the nuclear and electronic contributions. In the velocity range $v \sim 0.1v_0$ to $Z_1^{2/3}v_0$ the electronic energy loss is approximately proportional to velocity v or $E^{1/2}$.

At higher velocities, the charge state of the ion increases and ultimately becomes fully stripped of all its electrons at $v \geq v_0 Z_1^{2/3}$. At this point, the ion can be viewed as a positive point charge, Z_1, moving with a velocity greater than the mean orbital velocity of the atomic electrons in the shells or subshells of the target atom. When the projectile velocity v is much greater than that of an orbital electron (fast-collision case), the influence of the incident particle on an atom may be regarded as a sudden, small external perturbation. This picture leads to Bohr's theory of stopping power. The collision produces a sudden transfer of energy from the projectile to the target electron. The energy loss from a fast particle to a stationary nucleus or electron can be calculated from scattering in a central force field. The stopping cross section decreases with increasing velocity because the particle spends less time in the vicinity of the atom. In this high-energy, fast-collision regime, the values of electronic stopping are proportional to $(Z_1/v)^2$.

4.4.1 EFFECTIVE CHARGE OF MOVING IONS

As shown in Figure 4.2, the two regimes of electronic stopping are determined by the projectile's state of ionization or its effective charge. Bohr suggested that energetic ions would lose electrons whose orbital velocities were less than the ion velocity. Based on the Thomas–Fermi picture of the atom,

Bohr suggested that the ion charge fraction, or the effective ion charge, should be given by

$$\frac{Z^*}{Z} = \left(\frac{v}{v_0 Z_1^{2/3}}\right) \tag{4.5}$$

where
Z is the total number of electrons that would surround the ion in its ground state (i.e., the atomic number)
Z^* is the positive charge on the ion
v is the ion velocity
v_0 is the Bohr velocity of an electron in the innermost orbit of a hydrogen atom (i.e., $v_0 \cong 2.2 \times 10^8$ cm/s).

The difference, $Z - Z^*$, is the number of electrons remaining on the ion. From Figure 4.2 and Equation (4.5), we have two extreme states for an energetic ion:

$$v < v_0 Z_1^{2/3}$$

which implies that $Z^*/Z < 1$, that the ion is not fully stripped, and that

$$v > v_0 Z_1^{2/3}$$

implying that $Z^*/Z \cong 1$ and that the ion is fully stripped to a bare nucleus.

Experimentally, it has been found that the ion charge fraction for heavy ions (i.e., $Z > Z_{He}$) more closely follows the form

$$\frac{Z^*}{Z} = 1 - \exp\left[-0.92\, v \Big/ \left(v_0 Z_1^{2/3}\right)\right] \tag{4.6}$$

which expands approximately to the Bohr relation given in Equation (4.5).

In the sections that follow, we will derive electronic energy loss expression in the high-velocity regimes where the ion is fully stripped.

4.4.2 HIGH-ENERGY ELECTRONIC ENERGY LOSS

In this section we will consider the case where the ion velocity is greater than $v_0 Z_1^{2/3}$. For this condition, the ion is a bare nuclei, and its interactions with target electrons can be accurately described by a pure Coulomb interaction potential.

In 1913, Bohr derived an expression for the rate of energy loss of a charged particle on the basis of classical considerations. He considered a heavy particle, such as an α particle or a proton, of charge $Z_1 e$, mass M, and velocity v passing a target-atom electron of mass m_e at a distance b (Figures 4.3 and 4.4). As the heavy particle passes, the Coulomb force acting on the electron changes direction continuously. If the electron moves negligibly during the passage of the heavy particle, the impulse parallel to the path, $\int F dt$ is zero by symmetry,

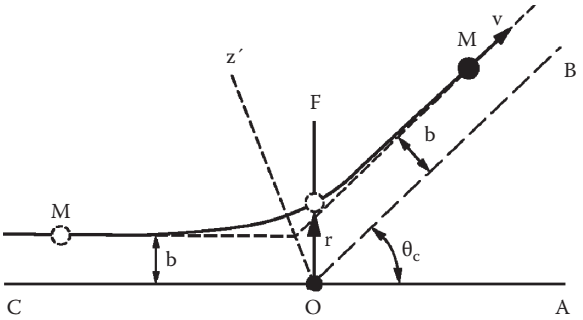

FIGURE 4.3 The nucleus is assumed to be a point charge at the origin O. At any distance r, the particle experiences a repulsive force. The particle travels along a path that is initially parallel to line OA, a distance b from it, and finally parallel to line OB, which makes an angle θ_c with OA.

since for each position of the incident particle in the –x direction there is a corresponding position in the +x direction that makes an equal and opposite contribution to the x component of the momentum. However, throughout the passage, there is a force in the y direction, and momentum Δp is transferred to the electron. This problem is identical to the momentum approximation introduced in Appendix 4.1 at the end of the chapter, where the momentum transferred to the target-atom electron is given by Equation (4.29) as

$$\Delta p = -\frac{1}{v}\frac{d}{db}\int_{-\infty}^{\infty} V\left(\left(x^2 + b^2\right)^{1/2}\right) dx \tag{4.7}$$

where
v is the ion velocity
b is the impact parameter
x is the distance along the ion's trajectory to the point r_{min}
$(x^2 + b^2)^{1/2}$ is the separation distance r between the ion and the electron (see Figure 4.4).
V is the interaction potential.

The interaction potential for this collision is purely Coulombic:

$$V(r) = \frac{Z_1 Z_2 e^2}{r}$$

or, in terms of $r = (x^2 + b^2)^{1/2}$,

$$V\left((x^2 + b^2)^{1/2}\right) = \frac{Z_1 Z_2 e^2}{(x^2 + b^2)^{1/2}} \tag{4.8}$$

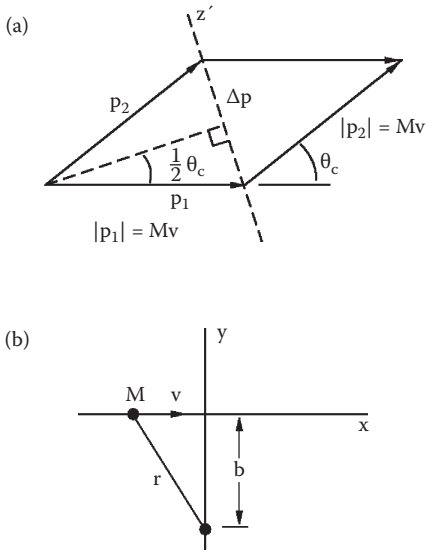

FIGURE 4.4 (a) Momentum diagram for impulse scattering (see Figure 4.3). Note that $|\mathbf{p}_1| = |\mathbf{p}_2|$ (i.e., for elastic scattering, the energy and speed of the projectile are the same before and after the collision). (b) Change-of-variable diagram for momentum (impulse) approximation.

Taking the derivative of the potential with respect to b,

$$-\frac{d}{db}\left(\frac{Z_1 Z_2 e^2}{\left(x^2 + b^2\right)^{1/2}}\right) = b\frac{Z_1 Z_2 e^2}{\left(x^2 + b^2\right)^{3/2}} \tag{4.9}$$

This allows us to write the momentum transferred to the electron during full passage of the ion as

$$\Delta p = \frac{Z_1 Z_2 e^2}{v b}\int_{-\infty}^{\infty}\frac{b^2\,dx}{\left(x^2 + b^2\right)^{3/2}} = \frac{2Z_1 Z_2 e^2}{v b} \tag{4.10}$$

which is appropriate for glancing collisions (i.e., $\theta \cong 0$). If the electron has not achieved a relativistic velocity, and noting that $Z_2 = 1$, the electron kinetic energy following the collision will be

$$T = \frac{\Delta p^2}{2m_e} = \frac{2Z_1^2 e^4}{b^2 m_e v^2} \tag{4.11}$$

where m_e is the electron mass and T is the energy transferred to the electron and lost by the ion in the collision.

The energy loss per unit path length, dE/dx, is

$$-\left.\frac{dE}{dx}\right|_e = n_e \int_{T_{min}}^{T_M} T \frac{d\sigma(E)}{dT}\, dT \tag{4.12}$$

where n_e is the number of electrons per unit volume. The differential cross section, $d\sigma(T)$, for an energy transfer between T and dT is

$$d\sigma(T) = -2\pi b\, db \tag{4.13}$$

This allows us to rewrite Equation (4.12) in terms of the impact parameter b as

$$-\left.\frac{dE}{dx}\right|_e = n_e \int_{b_{min}}^{b_{max}} T\, 2\pi b\, db \tag{4.14}$$

Substituting Equation (4.11) into Equation (4.14) and carrying out the integration,

$$-\left.\frac{dE}{dx}\right|_e = \frac{4\pi Z_1^2 e^4 n_e}{m_e v^2} \ln \frac{b_{max}}{b_{min}} \tag{4.15}$$

To choose a meaningful value for b_{min}, we observe that if the heavy projectile collided head on with the electron, the maximum velocity transferred to a stationary electron would be 2v. The corresponding maximum kinetic energy transferred (for a nonrelativistic v) is $T_{max} = 2m_e v^2$. If this value of T_{max} is inserted into Equation (4.11), the corresponding b_{min} becomes

$$b_{min} = \frac{Z_1 e^2}{m_e v^2} \tag{4.16}$$

If b_{max} is allowed to become infinite, –dE/dx goes to infinity because of the contribution of an unlimited number of small energy transfers given to distant electrons. But the smallest energy an atomic electron can accept must be sufficient to raise it to an allowed excited state. If I represents the average excitation energy of an electron, we choose $T_{min} = I$ and find

$$b_{max} = \frac{2Z_1 e^2}{\sqrt{2 m_e v^2 I}} \tag{4.17}$$

When Equations (4.15) and (4.16) are substituted into Equation (4.14), we obtain

$$-\left.\frac{dE}{dx}\right|_e = \frac{2\pi Z_1^2 e^4 n_e}{m_e v^2} \ln \frac{2 m_e v^2}{I}. \tag{4.18}$$

This calculation is based on direct collisions with electrons in the solid. There is another term of comparable magnitude due to distant resonant energy transfer. The full derivation leads to a total stopping power of twice that shown before—that is,

$$-\left.\frac{dE}{dx}\right|_e = \frac{4\pi Z_1^2 e^4 n_e}{m_e v^2} \ln \frac{2 m_e v^2}{I} \tag{4.18a}$$

or

$$-\left.\frac{dE}{dx}\right|_e = \frac{2\pi Z_1^2 e^4}{E} N Z_2 \left(\frac{M_1}{m_e}\right) \ln \frac{2 m_e v^2}{I} \tag{4.18b}$$

where $E = M_1 v^2/2$ and $n_e = NZ_2$, with N given by the atomic density in the stopping medium.

Thus, we can regard the electronic interactions as being composed of two contributions: (1) close collisions with large momentum transfers, where the particle approaches within the electronic orbits; and (2) distant collisions with small momentum transfers, where the particle is outside the orbits.

The average excitation energy I, in electron volts, for most elements is roughly $I \cong 10Z_2$, where Z_2 is the atomic number of the stopping atoms. Experimental and calculated values of I are given in Figure 4.5. The description of stopping power

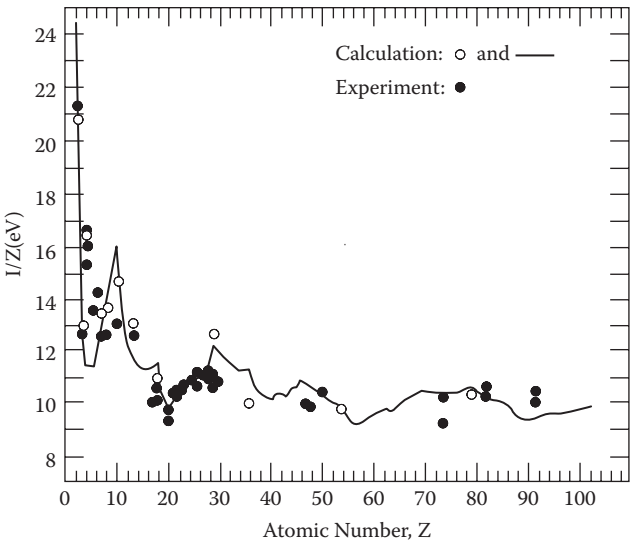

FIGURE 4.5 Calculation of mean excitation energy by Lindhard and Scharff's theory with a Hartree–Fock–Slater charge distribution. The calculation I/Z versus atomic number Z reveals structure, as was observed in many experimental measurements. (From Chu, W.- K. and Powers, D. 1972. *Physics Letters* 40A:23.)

so far ignores the shell structure of the atoms and variations in electron binding. Experimentally, these effects show up as small deviations (except for the very light elements) from the approximation given by $I \cong 10Z_2$, as shown in Figure 4.5.

The complete energy loss formula (often referred to as the Bethe formula) contains corrections that include relativistic terms at high velocities and corrections for the nonparticipation of the strongly bound inner shell electrons. For ions with $Z \geq Z_{He}$ in the energy regime of a few megaelectron volts, relativistic effects are negligible, and nearly all the target electrons participate ($I_e = NZ_2$) in the stopping process. Consequently, Equation (4.17) can be used to estimate values of $dE/dx\big|_e$.

For example, the electronic energy loss of 2 MeV ^{4}He ions in Al has a value (calculated from Equation 4.17) of 315 eV/nm using values of $n_e = NZ_2 = 780/nm^3$ and $I = 10Z_2 = 130$ eV. Experiments give a value of $dE/dx\big|_e = 266$ eV/nm. Thus, the first-order treatment gives values to within 20% of the experimental values.

4.5 STOPPING CALCULATIONS USING SRIM

The energy loss rate, dE/dx, can be calculated using the computer program "stopping and ion ranges in matter" (SRIM) (http://www.srim.org/). SRIM is a group of programs that calculate the stopping and range of ions (up to 2 GeV/amu) into matter using a quantum mechanical treatment of ion–atom collisions (assuming a moving atom as an ***ion*** and all target atoms as ***atoms***). This calculation is made very efficient by the use of statistical algorithms, which allow the ion to make jumps between calculated collisions and then average the collision results over the intervening gap. During the collisions, the ion and atom have a screened Coulomb collision, including exchange and correlation interactions between the overlapping electron shells. The ion has long-range interactions creating electron excitations and plasmons within the target. The charge state of the ion within the target is described using the concept of effective charge, which includes a velocity dependent charge state and long-range screening due to the collective electron sea of the target. A full description of the calculation is found in the tutorial book, *SRIM—The Stopping and Range of Ions in Solids,* by J. F. Ziegler and J. P. Biersack in 1985 (a new edition was published in 2008).

Examples of the stopping data provided by SRIM are given in Table 4.1 for He ions in Si at energies between 10 keV and 10 MeV.

4.6 ENERGY LOSS IN COMPOUNDS—BRAGG'S RULE

The process by which a particle loses energy when it moves swiftly through a medium consists of a random sequence of independent encounters between the moving projectile and the electrons attached to an atom of the solid. For a target that contains more then one element, the energy loss can be estimated by

TABLE 4.1 SRIM Stopping Data for He Ions in Si

Ion Energy	$[dE/dx]_e$ (eV nm^{-1})	$[dE/dx]_n$ (eV nm^{-1})
10.00 keV	53.63	10.29
25.00 keV	89.19	6.402
50.00 keV	138.0	4.155
100.00 keV	206.2	2.575
200.00 keV	283.0	1.541
300.00 keV	318.7	1.127
400.00 keV	333.4	0.898
500.00 keV	337.0	0.751
600.00 keV	334.5	0.648
700.00 keV	328.8	0.572
800.00 keV	321.3	0.513
900.00 keV	313.1	0.465
1.00 MeV	304.6	0.427
1.50 MeV	264.8	0.304
2.00 MeV	233.3	0.239
2.50 MeV	208.9	0.197
3.00 MeV	189.7	0.169
3.50 MeV	174.1	0.148
4.00 MeV	161.3	0.132
4.50 MeV	150.5	0.119
5.00 MeV	141.4	0.109
5.50 MeV	133.4	0.100
6.00 MeV	126.5	0.093
6.50 MeV	120.3	0.086
7.00 MeV	114.9	0.081
8.00 MeV	105.6	0.072
9.00 MeV	97.58	0.065
10.00 MeV	90.17	0.059

the sum of the losses of the constituent elements weighted by the abundance of the elements. This postulate is known as Bragg's rule and states that the stopping cross section $\varepsilon^{A_mB_n}$ of a solid of composition A_mB_n is given by

$$\varepsilon^{A_mB_n} = m\varepsilon^A + n\varepsilon^B \tag{4.19}$$

where ε^A and ε^B are the stopping cross sections of the atomic constituents A and B.

To take the specific example of SiO_2 on a molecular basis,

$$\varepsilon^{SiO_2} = \varepsilon^{Si} + 2\varepsilon^O$$

where ε^{SiO_2} is now the stopping power/molecule, so $dE/dX = N\,\varepsilon^{SiO_2}$ (see Equation 4.3), where N is the number of molecules/volume. Figure 4.6 shows the stopping cross section for SiO_2 on molecular basis.

4.7 ELECTRONIC ENERGY STRAGGLING

An energetic particle that moves through a medium loses energy via many individual encounters. These encounters slow the particle down and result in spreading the energy distribution of the particles. This phenomenon is called energy straggling, Ω_B. As a result, identical energetic particles, which have the same initial energy, do not have exactly the same energy after passing through a thickness Δt of a homogeneous medium.

Light particles such as H and He in the MeV energy range lose energy primarily by encounters with electrons in the target, and the dominant contribution to energy straggling is the statistical fluctuations in these electronic interactions. The straggling of the two-particle energy loss (the projectile and a stationary electron) is defined as

$$\Omega_B^2 = < T^2 > \tag{4.20}$$

where T is the energy loss by the projectile to the electron and $<T^2>$ is the mean squared average energy transferred.

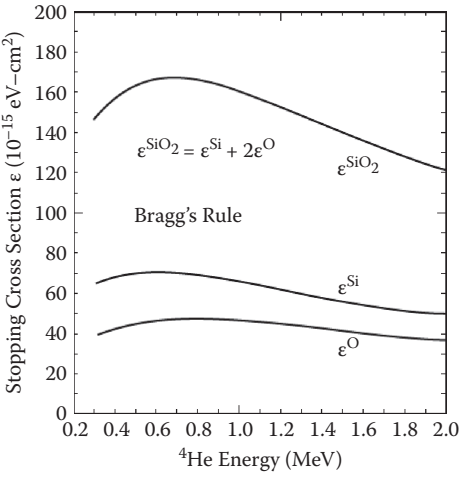

FIGURE 4.6 Stopping cross sections for He ions on Si, O, and SiO_2. The SiO_2 stopping cross section ε^{SiO_2} was determined on the molecular basis with 2.3×10^{22} molecules/cm^3.

The probability of a particle with energy E undergoing a collision with an electron while traveling a distance Δt that results in an energy loss between T and T + dT is given by

$$P(T) = n_e \Delta t \frac{d\sigma}{dT} \tag{4.21}$$

where E is the energy of the moving particle, n_e is the number of electrons per unit volume, and σ is the cross section defined by Equation (3.4) in Chapter 3, $d\sigma = 2\pi b\, db$, where b is the impact parameter.

The average energy transferred by the moving particle in the distance Δt is obtained by multiplying Equation (4.21) by the transfer energy T and integrating over all possible values of T (see Equation 4.11):

$$\langle T \rangle = \int T\ P(T)\ dT = n_e \Delta t \int_{T_{min}}^{T_M} T\ d\sigma \tag{4.22}$$

Similarly, the mean squared average energy transferred is given by

$$\langle T^2 \rangle \equiv \Omega_B^2 = n_e \Delta t \int_{T_{min}}^{T_M} T^2\, d\sigma = 2\pi N Z_2 \Delta t \int_{b_{max}}^{b_{min}} T^2\, b\, db \tag{4.23}$$

where n_e was replaced with NZ_2, where N is the atomic density. The relationship between impact parameter and transferred energy is given by Equation (4.11). The integral thus yields

$$\Omega_B^2 = 2\pi N Z_2 \Delta t \frac{(Z_1 e^2)^2}{m_e v^2} (T_{max} - T_{min}) \tag{4.24}$$

where T_{max} and T_{min} are energies transferred corresponding to encounters with minimum and maximum impact parameters b_{min} and b_{max}, respectively. The largest energy transfer in a collision between the ion of mass M_1 and an electron of mass $m_e \ll M_1$ is $2m_e v^2$; thus, for $T_{min} \ll T_{max}$, we have

$$\Omega_B^2 = 4\pi Z_1^2 e^4 N Z_2 \Delta t \tag{4.25}$$

This expression was first derived by Bohr (1915) and is often referred to as the *Bohr value of electronic energy straggling.* Described by Equation (4.25), Ω_B is usually referred to as the standard deviation of the ion energy distribution after passing through a medium of thickness Δt. The full width at half maximum

(FWHM) of the ion energy distribution, typically described by a normal or Gaussian function in most cases, would be calculated by

$$\text{FWHM} = 2\sqrt{2\ln 2}\Omega_B = 2.355\Omega_B$$

Bohr's theory predicts that the electronic energy straggling does not depend on the energy of the projectile and that the value of the energy variation increases with the square root of the number of electrons per unit area $NZ_2\Delta t$ in the target. A discussion of corrections to Bohr's theory of straggling can be found in Rauhala and Ziegler (2009).

The importance of straggling will become more apparent in the following chapters because energy straggling sets a fundamental limit to the depth resolution possible for ion beam energy loss techniques. For example, the amount of target material Nt (atoms/square centimeters) needed to produce 15 keV (FWHM) of energy straggling in Si with He ions is ~2.80×10^{18} atoms/cm^2, or 560 nm. In this example we have used the relationship FWHM = $2.355\Omega_B$ and $N_{si} = 5 \times 10^{22}$ atoms/cm^3.

PROBLEMS

4.1. Calculate the velocity, v, the Thomas–Fermi screening length a_{TF}, and the reduced energy ε, for 0.1, 1, and 10 MeV He ions incident on Ge.

4.2. Show that, for a proton of velocity v in a direct head-on collision with a stationary electron, the maximum change in energy of the electron is 2 $m_e v^2$. What is the change in velocity of the target proton for a head-on collision with an incident proton?

4.3. (a) What is the effective charge for 100 keV and 10 MeV Ar in Cu? (b) What is the effective charge for 100 keV and 10 MeV He in Si?

4.4. At what velocity are the following ions fully stripped: H, He, C, Si, Ar, Xe, and Au?

4.5. (a) In the electronic stopping high-velocity regime, what is the value of $dE/dx|_e$ for 10 MeV Ar in Cu according to Equation (4.17)? (b) Is 10 MeV Ar in the high-velocity, fully stripped regime? (c) How does this compare to the stopping result from SRIM?

4.6. What is the Bohr straggling for He in 50, 100, and 1000 nm of Au?

4.7. What is the thickness of Au that can be analyzed before it becomes comparable to a detector resolution of 20 keV (FWHM)? Perform the calculation for ions of H, He, and C.

4.8. What is the interatomic potential for He ions in silicon at 1/10 the atomic spacing?

4.9. What is the value of the minimum impact parameter for 1 MeV He ions and 1 MeV protons?

APPENDIX 4.1: THE CLASSICAL IMPULSE APPROXIMATION TO THE SCATTERING INTEGRAL

In this appendix we will examine the relationship between the potential V(r) and the scattering angle θ_c for the collisions where $V(r)/E_c$ remains small throughout the entire collision process. This condition is realized for collisions where b is large, which in turn leads to small-angle scattering.

The scattering cross section for central force scattering with large impact parameters can be calculated for small deflections from the impulse imparted to the particle as it passes the target nucleus. As the particle with charge Z_1e approaches the target nucleus, charge Z_2e, it will experience a repulsive force that will cause its trajectory to deviate from the incident straight line path (see Figure 4.3).

Let $\mathbf{p}_1$ and $\mathbf{p}_2$ be the initial and final momentum vectors of the particle. From Figure 4.4(a) it is evident that the total change in momentum, $\Delta\mathbf{p} = \mathbf{p}_2 - \mathbf{p}_1$, is along the z′ axis, which is the axis corresponding to the condition $r = r_{min}$. In this calculation the magnitude of the momentum does not change. From the isosceles triangle formed by $\mathbf{p}_1$, $\mathbf{p}_2$, and $\Delta\mathbf{p}$ shown in Figure 4.4(a) we have

$$\frac{\frac{1}{2}\Delta\mathbf{p}}{M\,\mathbf{v}} = \sin\frac{\theta_c}{2}$$

or, in the limit of $\theta_c \ll 1$,

$$\frac{\Delta\mathbf{p}}{M\mathbf{v}} = \frac{\Delta(M\mathbf{v})}{M\mathbf{v}} \cong \theta_c \tag{4.25}$$

Equation (4.25) indicates that, at small deflections, θ_c can be thought of as being due to a small impulse, $\Delta\mathbf{p} = \Delta(M\mathbf{v})$, approximately perpendicular to the original direction of motion. This small-angle calculation is commonly called the *impulse* or *momentum approximation.*

The impulse approximation is appropriate for the small-angle large-impact parameter collisions that dominate the sequence of scatterings that determine the charged particle trajectory. In the impulse approximation the change in momentum is given by

$$\Delta\mathbf{p} = \int_{-\infty}^{\infty} \mathbf{F}_0\, dt \tag{4.26}$$

or

$$\Delta\mathbf{p} = \frac{1}{\mathbf{v}}\int_{-\infty}^{\infty} \mathbf{F}_0\, dx \tag{4.27}$$

where $\mathbf{F}_0$ is the component of the force acting on the ion perpendicular to its incident direction. By using the geometry of Figure 4.4(b), the force may be written with $r = (x^2 + b^2)^{1/2}$ as

$$\mathbf{F}_0 = -\frac{dV(r)}{dy} = -\frac{dV\left(\left(x^2 + b^2\right)^{1/2}\right)}{db} \tag{4.28}$$

Then,

$$\Delta \mathbf{p} = -\frac{1}{\mathbf{v}} \frac{d}{db} \int_{-\infty}^{\infty} V\left(\sqrt{x^2 + b^2}\right) dx \tag{4.29}$$

or, using Equation (4.25),

$$\theta_c = \frac{\Delta(\mathbf{Mv})}{\mathbf{Mv}} = -\frac{1}{2E} \frac{d}{db} \int_{-\infty}^{\infty} V(r)\, dx \tag{4.30}$$

for $\theta_c << 1$. Equation (4.30) shows that the angle θ_c is obtained from the potential V(r) by one integration followed by one differentiation. Using $r = (x^2 + y^2)^{1/2}$ to change the integration variable in Equation (4.30) yields

$$\theta_c = \frac{1}{E_c} \int_{b}^{\infty} \left(\frac{dV}{dr}\right) \frac{b}{r} \left[1 - \left(\frac{b}{r}\right)^2\right]^{-1/2} dr \tag{4.31}$$

Equation (4.31) is often referred to as the classical impulse approximation to the scattering integral.

REFERENCES

Bohr, N. 1915. Decrease of speed of electrified particles in passing through matter. *Philosophical Magazine* 30:581.

Chu, W-. K., and Powers, D. 1972. Calculation of mean excitation energy for all elements. *Physics Letters* 40A:23.

Nastasi, M., Mayer, J. W., and Hirvonen, J. 1996. *Ion–solid interactions: Fundamentals and applications.* Cambridge: Cambridge University Press.

Rauhala, E., and Ziegler, J. F. 2009. Energy loss and energy straggling. In *Handbook of modern ion beam materials analysis,* 2nd ed., eds. Y. Wang and M. Nastasi, chap. 2. Warrendale, PA: Materials Research Society.

Ziegler, J. F., Biersack, J. P., and Ziegler, M. D. 2008. *The stopping and range of ions in matter,* chap. 6. Chester, MD: SRIM Co.

SUGGESTED READING

Alford, T. L., Feldman, L. C., and Mayer, J. W. 2007. *Fundamentals of nanoscale film analyses,* chap. 3. New York: Springer.

Chu, W.-K, Mayer, J. W., and Nicolet, M.-A. 1978. *Backscattering spectrometry,* chap. 2. New York: Academic Press.

Gotz, G., and Gartner, K. eds. 1988. In *High energy ion beam analysis of solids,* chap. 1. Berlin: Academie Verlag.

Ziegler, J. F., Biersack, J. P., and Littmark, U. 1985. *The stopping and range of ions in solids,* vol. 1. New York: Pergamon Press.

Backscattering Spectrometry

5

5.1 INTRODUCTION

Backscattering spectrometry is a method that provides accurate depth information (typically, accuracies of a few percent, with 10–30 nm in depth resolution) about the stoichiometry, elemental area density, and impurity distributions in the near surface region of bulk materials and in thin films. Detection limits range from about a few parts per million for heavy elements to a few percent for light elements. Analysis depths using He ions are typically a few thousand nanometers. Depth profile information is obtained in a nondestructive manner. The results obtained typically do not require the use of standards and are insensitive to the sample chemical bonding. In addition, it is a quick and easy experiment to perform, typically with data acquisition times of a few tens of minutes.

The majority of backscattering analyses have been performed with ^{4}He ions in the 1–2 MeV range. The reasons for this include: (1) the backscattering cross section of ^{4}He incident on all elements with mass greater than Be is nearly Rutherford in this range (see Figure 3.6 in Chapter 3), (2) experimental and semiempirical data for energy loss are reasonably well known, and (3) accelerators that produce ions at these energies are more abundant.

5.2 EXPERIMENTAL SETUP

Backscattering spectrometry is based on collisions between an energetic incident ion and a target nucleus. The probability of a collision resulting

in a backscattered event is related to the collision cross section discussed in Chapter 3. If the interaction between the incident particle and target nuclei can be described by Coulombic forces, the scattering is defined as *Rutherford,* which derives its name from Lord Ernest Rutherford, who first presented the concept of atoms having nuclei. For Rutherford backscattering, the scattering cross section is defined by Equation (3.22) in Chapter 3. The scattering cross section along with the kinematics (see Chapter 2) of the collision is independent of chemical bonding, making the backscattering measurement insensitive to matrix effects.

The experimental setup for a backscattering experiment is shown in Figure 5.1(a). A collimated beam of monoenergetic He ions is incident on a planar sample. Particles (He) backscattered to an angle θ are detected by a detector of solid angle Ω (Equation 3.1). In the most typical applications, all of the apparatus are under vacuum. Figure 5.1(b) shows a schematic representation of the elastic collision between the incident projectile of mass M_1 and energy E_0 and a target of mass M_2, which is initially at rest. After the collision, the projectile and target mass have energies of E_1 and E_2 and have been scattered to the laboratory angles θ and ϕ, respectively.

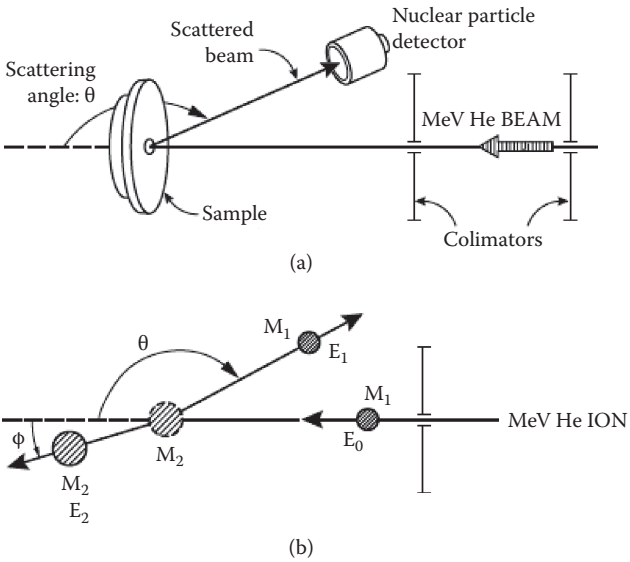

FIGURE 5.1 (a) Schematic of the experimental setup of a backscattering experiment. (b) Schematic representation of the collision process that takes place in the sample depicted in the experimental setup shown in (a).

5.3 ENERGY LOSS AND DEPTH SCALE

The energy loss by the incident projectile during the collision is defined by the kinematic factor K given in Equation (2.9) in Chapter 2. As discussed in that chapter, it is the loss of energy during the collision process that allows backscattering spectrometry to detect different masses in the target. The energy loss dE/dx by the projectile as it traverses the specimen will allow us to extract depth information from the sample.

In addition to energy losses during collisions, the incident particles will also lose energy as they travel into the target before the collision and out of the target after the collision. This process is schematically shown in Figure 5.2. To a good approximation, the total energy loss ΔE_{in} into a depth, t, before the collision is proportional to t. That is,

$$\Delta E_{in} = \int_0^{t/\cos\theta_1} \left.\frac{dE}{dx}\right|_{in} dx \cong \frac{t}{\cos\theta_1} \left.\frac{dE}{dx}\right|_{in} \tag{5.1}$$

where $\left.dE/dx\right|_{in}$ is evaluated at some average energy between the incident energy E_0 and $E_0 - \Delta E_{in}$. This is the energy loss component that arises from the projectile incident at an angle θ_1 degrees away from the surface normal after traversing a thickness t. Thus, the energy of the incident particle just prior to the collision at depth t is

$$E_t = E_0 - \Delta E_{in} \tag{5.2}$$

After scattering, the projectile has a reduced energy of KE_t. Therefore, the energy loss by the projectile during the scattering process at depth t is

$$\Delta E_s = E_t - KE_t = (1 - K)E_t \tag{5.3}$$

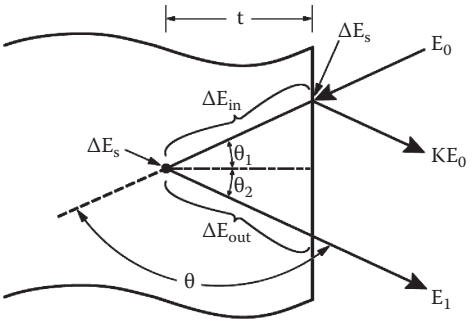

FIGURE 5.2 The energy loss components for a projectile scattered from a depth, t, in a single element target.

The energy loss on the outward path for a particle scattered θ_2 degrees away from the surface normal of the sample is given by

$$\Delta E_{out} = \int_0^{t/\cos\theta_2} \left.\frac{dE}{dx}\right|_{out} dx \cong \frac{t}{\cos\theta_2} \left.\frac{dE}{dx}\right|_{out} \tag{5.4}$$

The energy E_1 is the energy measure at the detector and is given by

$$E_1 = E_0 - (\Delta E_{in} + \Delta E_s + \Delta E_{out}) = KE_t - \Delta E_{out} \tag{5.5}$$

Alternately, if the projectile is scattered from the surface without penetrating the solid, the only energy loss will be due to kinematics and the detected projectile energy will be KE_0.

The total energy difference ΔE between projectiles scattered at the surface and at some depth t is thus given by

$$\Delta E = KE_0 - E_1 = K\Delta E_{in} - \Delta E_{out} \equiv [S]\ t = N[\varepsilon]\ t \tag{5.6}$$

where [S] is the energy loss factor, [ε] is the stopping cross-section factor, and N is the atomic density. The energy loss factor can be defined from Equations (5.1)–(5.6) as

$$[S] \equiv \left[\frac{K}{\cos\theta_1} \left.\frac{dE}{dx}\right|_{in} + \frac{1}{\cos\theta_2} \left.\frac{dE}{dx}\right|_{out} \right] \tag{5.7}$$

where the subscripts "in" and "out" refer to energies at which dE/dx is evaluated, and the stopping cross-section factor is defined as

$$[\varepsilon] \equiv \left[\frac{K}{\cos\theta_1} \varepsilon_{in} + \frac{1}{\cos\theta_2} \varepsilon_{out} \right] \tag{5.8}$$

where ε is the stopping cross section defined in Equation (4.4) in Chapter 4 as

$$\varepsilon \equiv \frac{1}{N} \frac{dE}{dx} \tag{5.9}$$

Equations (5.7) and (5.8) are derived assuming that dE/dx or ε is constant along the inward and outward paths. This assumption leads to a linear relation between ΔE and the depth, t, at which scattering occurs. One can therefore assign a linear depth to the energy axis, as indicated in Figure 5.3.

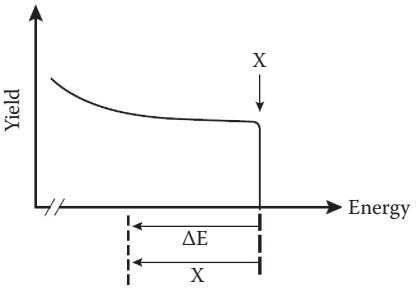

FIGURE 5.3 If the energy loss is assumed to be constant along the inward and outward paths, then the energy ΔE can be linearly related to the depth x through ΔE = [S]x, as indicated in the abscissa of the backscattering spectrum.

5.3.1 SURFACE ENERGY AND MEAN ENERGY APPROXIMATION

For thin films with a thickness ≤ 100 nm, the relative change in energy along the paths is small. For these conditions, the evaluation of dE/dx can be carried out using the "surface energy approximation" in which $dE/dx|_{in}$ is evaluated at E_0 and $dE/dx|_{out}$ is evaluated at KE_0. In this approximation we have

$$[S_0] \equiv \left[\frac{K}{\cos\theta_1} \frac{dE}{dx}\bigg|_{E_0} + \frac{1}{\cos\theta_2} \frac{dE}{dx}\bigg|_{KE_0} \right] \tag{5.10}$$

and

$$[\varepsilon_0] \equiv \left[\frac{K}{\cos\theta_1} \varepsilon(E_0) + \frac{1}{\cos\theta_2} \varepsilon(KE_0) \right] \tag{5.11}$$

When the path length becomes appreciable, the surface energy approximation breaks down. A better approximation can be obtained by selecting constant values of dE/dx at a mean energy $\bar{E}$ intermediate between the energy the particle has at the end points of each track. For these conditions we have

$$[\bar{S}] \equiv \left[\frac{K}{\cos\theta_1} \frac{dE}{dx}\bigg|_{\bar{E}_{in}} + \frac{1}{\cos\theta_2} \frac{dE}{dx}\bigg|_{\bar{E}_{out}} \right] \tag{5.12}$$

and

$$[\bar{\varepsilon}] \equiv \left[\frac{K}{\cos\theta_1} \varepsilon(\bar{E}_{in}) + \frac{1}{\cos\theta_2} \varepsilon(\bar{E}_{out}) \right] \tag{5.13}$$

The mean energy $\bar{E}$ can be estimated several ways. For the inward track, the particle enters at E_0 and has energy E_t (Equation 5.2) before scattering at

depth t so that $\overline{E}_{in} = \frac{E_t + E_0}{2}$. After scattering, the particle has energy KE_t, so that $\overline{E}_{out} = \frac{E_1 + KE_t}{2}$. The value of E_t is unknown, but can be estimated if the energy ΔE (Equation 5.6) can be measured. For a quick estimate it is assumed that ΔE is subdivided symmetrically between the inward and outward paths, so that E_t is approximately $E_0 - \frac{1}{2}\Delta E$. The values of $\overline{E}_{in}$ and $\overline{E}_{out}$ are then given by

$$\overline{E}_{in} \cong E_0 - \frac{1}{4}\Delta E \tag{5.14}$$

and

$$\overline{E}_{out} \cong E_1 + \frac{1}{4}\Delta E \tag{5.15}$$

5.3.2 COMPOUND TARGETS

For the situation where the target is composed of more than one element, the energy loss is assumed to be equal to the sum of the loss to the constituent elements, weighted by their abundance in the compound. This postulate is known as Bragg's rule, as discussed in Chapter 4. Thus, the stopping cross section for a mixture with the composition A_mB_n is given by Equation (4.19), $\varepsilon^{A_mB_n} = m\varepsilon^A + n\varepsilon^B$, where ε^A and ε^B are the stopping cross sections for elements A and B.

For compound targets similar energy losses will occur as those depicted in Figure 5.2, with the added complexity of kinematic losses from two elements. A schematic representation of the backscattering process from an idealized free-standing compound film is presented in Figure 5.4(a). The energy loss components that arise from a projectile traversing a thickness t and then being backscattered out for the A component are

$$\Delta E_{in}^{A_mB_n} = \frac{t}{\cos\theta_1}\left.\frac{dE}{dx}\right|_{in}^{A_mB_n} \tag{5.16}$$

$$E_t = E_0 - \Delta E_{in}^{A_mB_n} \tag{5.17}$$

$$\Delta E_s(A) = E_t - K_A E_t \tag{5.18}$$

$$\Delta E_{out}^{A_mB_n}(A) = \frac{t}{\cos\theta_2}\left.\frac{dE}{dx}\right|_{out,A}^{A_mB_n} \tag{5.19a}$$

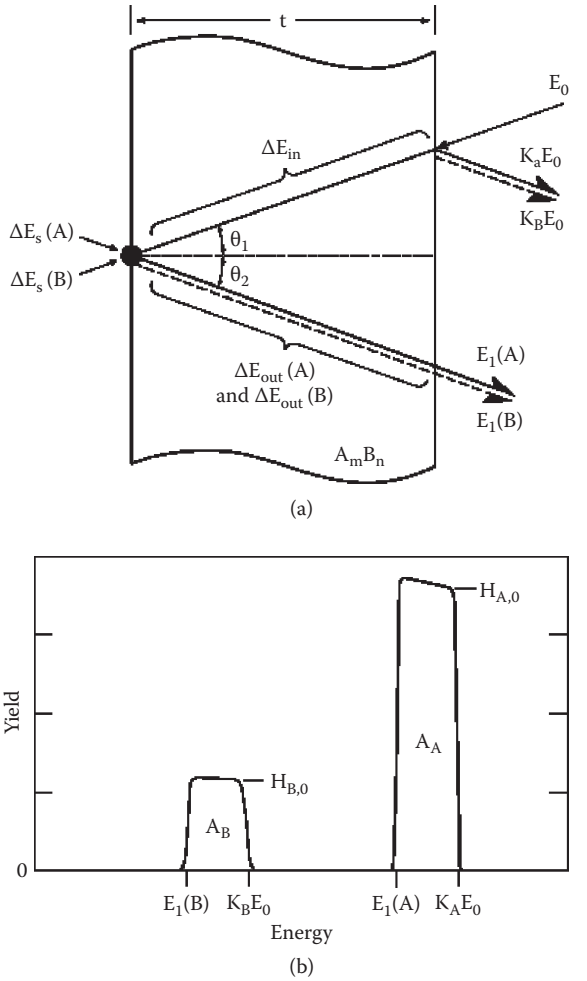

FIGURE 5.4 A schematic representation of the backscattering process from a free-standing compound film with composition A_mB_n and thickness t. (a) Energy loss relations, and (b) predicted backscattering spectrum.

Similar expressions exist for the B component of the compound target as

$$\Delta E_{out}^{A_mB_n}(B) = \frac{t}{\cos\theta_2}\left.\frac{dE}{dx}\right|_{out,B}^{A_mB_n} \tag{5.19b}$$

The relationship between the energy width, $K_AE_0 - E_1(A)$, and the scattering depth t is

$$\Delta E_A = K_AE_0 - E_1(A) \equiv t\ N^{A_mB_n}[\varepsilon]_A^{A_mB_n} \tag{5.20a}$$

and

$$\Delta E_B = K_B E_0 - E_1(B) \equiv t\, N^{A_mB_n} [\varepsilon]_B^{A_mB_n} \tag{5.20b}$$

where $N^{A_mB_n}$ is the number of molecules of A_mB_n per unit volume and $[\varepsilon]_A^{A_mB_n}$ ($[\varepsilon]_B^{A_mB_n}$) is the stopping cross-section factor for a projectile scattered from element A (B) while traversing the medium A_mB_n, and has the form

$$[\varepsilon]_A^{A_mB_n} = \left[\frac{K_A}{\cos\theta_1} \varepsilon_{in}^{A_mB_n} + \frac{1}{\cos\theta_2} \varepsilon_{out,A}^{A_mB_n} \right] \tag{5.21a}$$

and

$$[\varepsilon]_B^{A_mB_n} = \left[\frac{K_B}{\cos\theta_1} \varepsilon_{in}^{A_mB_n} + \frac{1}{\cos\theta_2} \varepsilon_{out,B}^{A_mB_n} \right] \tag{5.21b}$$

5.4 SCATTERING CROSS SECTION AND THE SHAPE OF THE BACKSCATTERING SPECTRUM

In the preceding discussion we assumed that collisions would occur between the projectile and a target atom that would result in a backscattering event. The likelihood of such an occurrence leads to the concept of the scattering cross section (Chapter 3) and the ability of performing quantitative composition analysis. The energy spectrum from an infinitely thick target is schematically shown in Figure 5.5. The shape of the spectrum can be understood from the relationships developed between depth and energy loss in Section 5.3 and the energy dependence of the Rutherford cross sections, Equation (3.22). For convenience, the Rutherford cross-section formula is relisted here:

$$\frac{d\sigma(\theta)}{d\Omega} = \left(\frac{Z_1 Z_2 e^2}{4E} \right) \frac{4}{\sin^4\theta} \frac{\{[1 - ((M_1/M_2)\sin\theta)^2]^{1/2} + \cos\theta\}^2}{[1 - ((M_1/M_2)\sin\theta)^2]^{1/2}} \tag{5.22}$$

For the experimental conditions shown in Figure 5.5, where a uniform beam of projectiles impinges at normal incidence on a uniform target, the spectrum height or yield of backscattered particles detected from a thin layer of atoms (Δt) is

$$Y = \sigma(\theta)\, \Omega\, Q\, N\Delta t/\cos\theta_1 \tag{5.23}$$

where
$\sigma(\theta)$ is the scattering cross section at angle θ
Ω is the detector solid angle

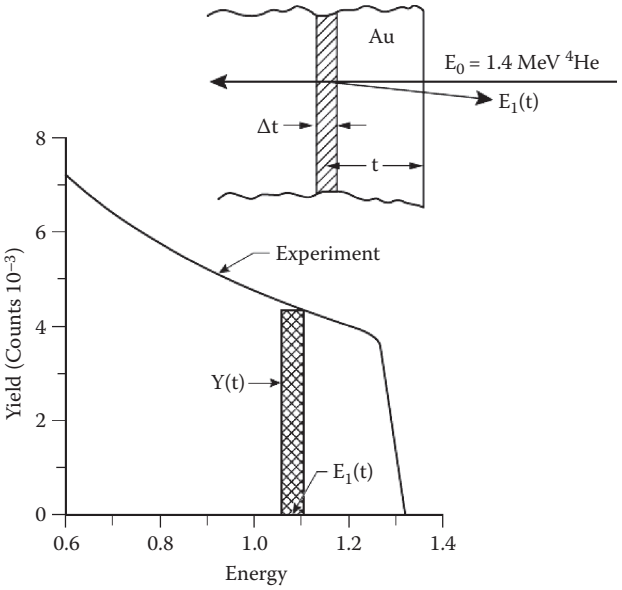

FIGURE 5.5 Backscattering spectrum for 1.4 MeV He ion incident on a thick Au sample.

Q is the measured number of incident particles
N is the atomic density, which makes NΔt the number of target atoms per unit area in the layer Δt thick
θ_1 is the angle between the incident beam and the surface normal of the target

For thick targets, projectiles scatter from any depth t, resulting in a continuous energy spectrum starting at KE_0 and going down to low energy, as shown in Figure 5.5. The yield from a slice of materials Δt wide at depth t is given by (for $\theta = 180°$)

$$Y(t) = \sigma(E(t))\ \Omega\ Q\ N\Delta t/\cos\theta_1 \tag{5.24}$$

where $\sigma(E(t))$ is the scattering cross section when the particle has energy E(t), at depth t. Note: In Figure 5.5, θ_1 is set to 0.

For Rutherford scattering, using Equation (5.22), we can rewrite Equation (5.24) as

$$Y(t) \cong \left(\frac{Z_1 Z_2 e^2}{4E(t)}\right)^2 \Omega Q N \Delta t \propto \frac{1}{E(t)^2} \tag{5.25}$$

Therefore, under Rutherford scattering conditions the shape of the energy spectrum should vary as $1/E^2$. This causes an increase in signal height toward decreasing energy or deeper into the sample, as shown in Figure 5.5.

The shape of backscattering spectra and depth profiles can be obtained from computer programs used in both simulation and analysis of backscattering data. This will be discussed in more detail in Chapter 15.

5.5 COMPOSITION AND DEPTH PROFILES

Equations (5.23) and (5.24) show that when Ω, Q, and σ are known, the number of atoms per unit area, Nt, can be calculated. If the interaction between projectile and target atom is Coulombic, the cross section is easily calculated using the Rutherford formula, Equation (5.22). At higher energies, the probability that the interaction between the projectile and target atom is non-Rutherford increases (Chapter 3) and experimentally determined values of σ are required.

In the hypothetical situation of a free standing film with composition A_mB_n, as depicted in Figure 5.4, the total number of counts from element A is area A_A in Figure 5.4(b). Assuming that only small changes in the projectile energy (e.g., very thin films) occur on the inward and outward paths (surface energy approximation), the area A_A can be described by (Chu, Mayer, and Nicolet, 1978):

$$A_A = \Omega\, Q\, \sigma_A(E_0)\, mN^{A_mB_n}\, t/\cos\theta_1 \tag{5.26a}$$

where $\sigma_A(E_0)$ is the scattering cross section for A atoms under the surface energy approximation and $mN^{A_mB_n}$ is the atomic density of A atoms in the compound A_mB_n. A similar expression can be written for A_B using the scattering cross section for B atoms, $\sigma_B(E_0)$ and the atomic density of B atoms, $nN^{A_mB_n}$:

$$A_B = \Omega\, Q\, \sigma_B(E_0)\, nN^{A_mB_n}\, t/\cos\theta_1 \tag{5.26b}$$

By combining Equations (5.26a) and (5.26b), the ratio of the atomic densities of A and B atoms can be found to be

$$\frac{m}{n} \equiv \frac{N_A}{N_B} = \frac{A_A}{A_B}\frac{\sigma_B(E_0)}{\sigma_A(E_0)} \tag{5.27}$$

In some situations it may not be possible to resolve the full peak of a particular element in a backscattering spectrum. In this case Equation (5.27), which utilizes the ratio of peak areas, cannot be directly used for composition analysis. However, a composition analysis may be possible by comparing surface heights of the backscattering yield. In an analogous expression to Equation (5.26), the backscattering yield at the surface for elements A and B in Figure 5.4 is separately given by

$$H_{A,0} = \Omega Q\, \sigma_A(E_0)\, mN^{A_mB_n}\, \tau_{A,0}/\cos\theta_1 \tag{5.28a}$$

and

$$H_{B,0} = \Omega Q\ \sigma_B(E_0)\ nN^{A_mB_n}\ \tau_{B,0}/\cos\theta_1 \tag{5.28b}$$

where $\tau_{A,0}$ and $\tau_{B,0}$ are the corresponding thicknesses of a slab of the target at the surface for elements A and B and defined by the energy width ξ of a channel in the detecting system (typically a few kiloelectron volts per channel). Projectiles scattered from within $\tau_{A,0}$ and $\tau_{B,0}$ will have a depth scale at the surface given by

$$\xi = \tau_{A,0} N^{A_mB_n} [\varepsilon]_A^{A_mB_n} \tag{5.29a}$$

and

$$\xi = \tau_{B,0} N^{A_mB_n} [\varepsilon]_B^{A_mB_n} \tag{5.29b}$$

where $N^{A_mB_n}$ is the number of molecules of A_mB_n per unit volume and $[\varepsilon]_A^{A_mB_n}$ ($[\varepsilon]_B^{A_mB_n}$) is the stopping cross-section factor for a projectile scattered from element A (B) while traversing the medium A_mB_n. Combining Equations (5.28) and (5.29) gives

$$H_{A,0} = \frac{\Omega Q\ \sigma_A(E_0)\ m\xi}{[\varepsilon]_A^{A_mB_n} \cos\theta_1} \tag{5.30a}$$

and

$$H_{B,0} = \frac{\Omega Q\ \sigma_B(E_0)\ n\xi}{[\varepsilon]_B^{A_mB_n} \cos\theta_1} \tag{5.30b}$$

Combining these equations, the ratio of atomic densities for atoms A to B for a thick target can be written as

$$\frac{m}{n} \equiv \frac{N_A}{N_B} = \frac{H_{A,0}\ \sigma_B(E_0)[\varepsilon]_A^{A_mB_n}}{H_{B,0}\ \sigma_A(E_0)[\varepsilon]_B^{A_mB_n}} \tag{5.31}$$

5.6 EXAMPLES

In this section we will provide two examples of the types of analysis that can be carried out with backscattering spectrometry.

5.6.1 THIN FILM REACTION ANALYSIS

Figure 5.6 shows schematic Rutherford backscattering spectra for ^{4}He ions incident on a 100 nm thick Ni film on a Si substrate (a) in its as-deposited state and (b) after interdiffusion and thermal reaction. In the reaction between Ni and Si,

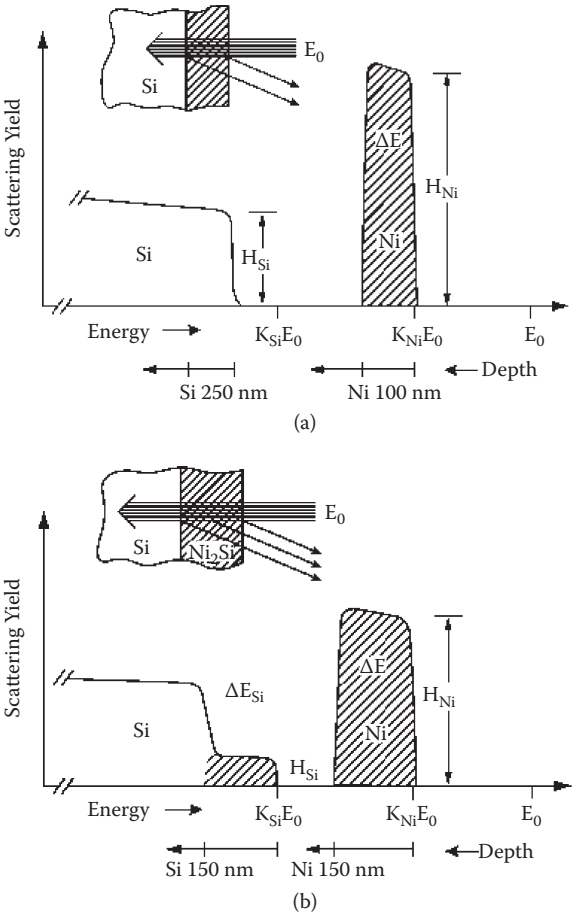

FIGURE 5.6 Schematic backscattering spectra for MeV ^{4}He ions incident on 100 nm Ni film on Si. (a) Before reaction, and (b) after reaction to form Ni_2Si.

the compound Ni_2Si is formed. Alpha particles scattered from the surface have an energy given by the kinematic equation $E_1 = KE_0$, where the kinematic factor for ^{4}He backscattered at a laboratory angle of 170° is 0.7624 for Ni and 0.5657 for Si.

As the alpha particles traverse the Ni film target, they lose energy at a rate of approximately 640 eV/nm along the incident path. A reasonable assumption in the limit of the surface energy approximation is that energy loss is linear with thickness. Thus, a 2 MeV ^{4}He ion will lose 64 keV penetrating the 100 nm Ni film before reaching the Si substrate. Immediately after scattering from a Ni atom at the interface, the ^{4}He will have an energy of 1.476 MeV. On the outward path, the scattered ^{4}He will have a slightly different energy loss due to the energy dependence of the energy loss process—approximately 690 eV/nm. The

scattered ^{4}He will also have a slightly longer path length ($t/\cos\theta_2$) reemerging to the surface where $\theta_2 = 10°$. Thus, the ^{4}He will emerge from the Ni surface with 1.406 MeV. The total energy difference between particles scattered form Ni atoms at the target surface and Ni atoms at the Ni/Si interface will be 119 keV, which can be derived from Equation (5.6).

The reaction between Ni and Si is shown in Figure 5.6(b). After the reaction the Ni energy signal ΔE_{Ni} has spread slightly due to the presence of Si atoms contributing to the energy loss. The Si has a step in its leading edge due to its reaction with Ni and the formation of Ni_2Si. As discussed for Equations (5.28)–(5.31), the ratio of the heights of Ni to Si, H_{Ni}/H_{Si}, from the Ni and Si peaks after silicide layer gives the composition of the layer. This can be calculated from Equation (5.31). In a first approximation we will note that $[\varepsilon_{Ni}^{Ni_2Si}] \approx [\varepsilon_{Si}^{Ni_2Si}]$, which allows us to obtain to within an accuracy of 5%–10%:

$$\frac{N_{Ni}}{N_{Si}} \cong \frac{H_{Ni}\ \sigma_{Si}(E_0)}{H_{Si}\ \sigma_{Ni}(E_0)} \tag{5.32}$$

If the scattering is Rutherford we can make use of the fact that $\sigma_{Si} \propto (Z_{Si})^2$ and $\sigma_{Ni} \propto (Z_{Ni})^2$, which allows us to write Equation (5.32) as

$$\frac{N_{Ni}}{N_{Si}} \cong \frac{H_{Ni}}{H_{Si}}\left(\frac{Z_{Si}}{Z_{Ni}}\right)^2 = \frac{H_{Ni}}{4H_{Si}} \tag{5.33}$$

A better approximation can be obtained by measuring the energy width of the Ni_2Si reaction layer in the Ni and Si peaks (hashed area in Figure 5.6b) and noting from Equation (5.6):

$$\Delta E_{Ni}^{Ni_2Si} = \Delta t\, N^{Ni_2Si}[\varepsilon]_{Ni}^{Ni_2Si} \tag{5.34a}$$

and

$$\Delta E_{Si}^{Ni_2Si} = \Delta t\, N^{Ni_2Si}[\varepsilon]_{Si}^{Ni_2Si} \tag{5.34b}$$

Substituting the stopping cross-section factors given in Equations (5.34a) and (5.34b) into Equation (5.31) leads to

$$\frac{N_{Ni}}{N_{Si}} = \frac{H_{Ni}\ \sigma_{Si}\ \Delta E_{Ni}^{Ni_2Si}}{H_{Si}\ \sigma_{Ni}\ \Delta E_{Si}^{Ni_2Si}} \tag{5.35}$$

In this case of Ni_2Si, the difference between application of Equations (5.32) and (5.35) corresponds to a 5% difference in the determination of the stoichiometry of the silicide.

5.6.2 ION IMPLANTATION

Figure 5.7 shows the RBS (Rutherford backscattering spectrometry) energy spectrum from 2.0 MeV ^{4}He ions backscattered from a silicon target implanted with ^{75}As at 250 keV to a fluence of 1.2×10^{15} As/cm^2. The Si signal gives a step with leading edge at 1.13 MeV, and the As signal (plotted on an amplified scale) has a Gaussian distribution with a peak at 1.55 MeV and a full width at half maximum (FWHM) of 60 keV. The As peak is shifted by $\Delta E_{As} = 68$ keV below the energy edge $K_{As}E_0 = 1.618$ MeV of the As at the surface. The data from Figure 5.7 are given in Table 5.1 (Chu et al. 1978)

Using Figure 5.7 and Table 5.1, we now proceed to calculate the implantation fluence, range, and range distribution for As in Si. We will assume that As is sufficiently shallow in Si that the surface energy approximation can be used to calculate the stopping cross section and Rutherford cross section. In calculating the As fluence, we use the backscattered Si signal as an internal calibration

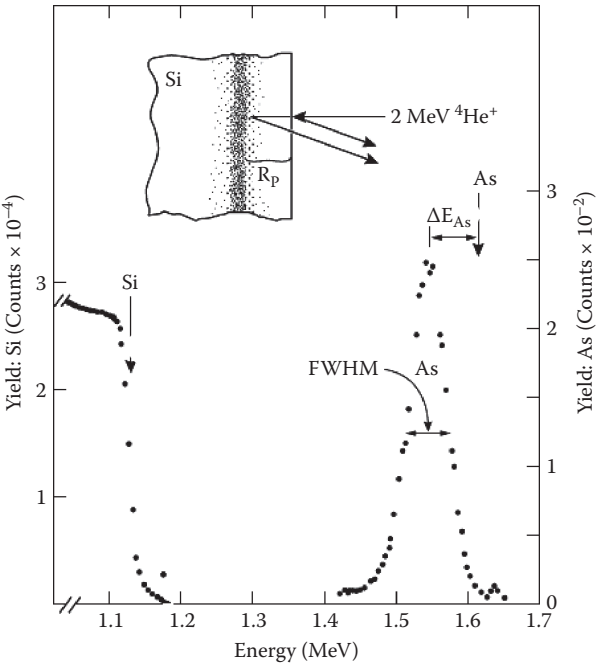

FIGURE 5.7 Energy spectrum of 2 MeV ^{4}He ions backscatterd from a silicon wafer implanted with 250 keV As ions to a nominal fluence of 1.2×10^{15} ions/cm^2. The vertical arrows indicate the energies of ^{4}He backscattered from surface atoms of ^{28}Si and ^{75}As.

TABLE 5.1 Data and Parameters Associated with Figure 5.7[a]

Data	Parameters
$H_{Si,0} = 27{,}000$ counts	$[\varepsilon_0]^{Si}_{Si} = 92.6 \times 10^{-15}$ eVcm^2
$H^{Si}_{As} = 250$ counts (at peak)	$[\varepsilon_0]^{Si}_{As} = 95.3 \times 10^{-15}$ eVcm^2
$A_{As} = 3{,}350$ counts	$\sigma_{As} = 1.425 \times 10^{-24}$ cm^2
$\Delta E_{As} = 68$ keV	$\sigma_{Si} = 0.248 \times 10^{-24}$ cm^2
$(FWHM)_{As} = 60$ keV	$K_{As} = 0.809$; $K_{Si} = 0.566$

[a] Based on the surface energy approximation. Values are $E_0 = 2.0$ MeV $^4He^+$ beam at normal incidence with $\theta = 170°$ and $\xi = 5.0$ keV.

and treat the implanted As as a dilute impurity in Si. That is, we will combine Equations (5.26) and (5.28) to yield

$$(Nt)_{As} = \frac{A_{As}}{H_{Si}} \frac{\sigma_{Si}(E_0)}{\sigma_{As}(E_0)} \frac{\xi}{[\varepsilon_0]_{Si}} = 1.2 \times 10^{15}\ \text{As/cm}^2 \tag{5.36}$$

This is in agreement with the nominal value of the implanted fluence.

The maximum concentration of As in Si can be estimated from the peak height of the As signal. Using Equation (5.31) and the data in Table 5.1 yields

$$\frac{N_{As}}{N_{Si}} = \frac{H_{As}}{H_{Si}} \frac{\sigma_{Si}(E_0)}{\sigma_{As}(E_0)} \frac{[\varepsilon_0]^{Si}_{As}}{[\varepsilon_0]^{Si}_{Si}} = 0.166\ \text{at.\%} \tag{5.37}$$

Using $N_{Si} = 5.00 \times 10^{22}$ atoms/cm^3 gives a value of $N_{As} = 8.30 \times 10^{19}$ atoms/cm^3.

To obtain the As concentration profile we first determine the As projected range, R_p. To calculate R_p we use Equation (5.6) and the stopping cross-section factor $[\varepsilon_0]^{Si}_{As}$, which gives the energy-to-depth conversion for scattering from As in a Si matrix. The peak position of arsenic is shifted by $\Delta E_{As} = 68$ keV below the As surface edge, and

$$R_p = \Delta E_{As} / (N_{Si}[\varepsilon_0]^{Si}_{As}) = 143\ \text{nm} \tag{5.38}$$

When the implanted distribution is Gaussian, the depth profile can be described by a projected range R_p and a range straggling ΔR_p, which is the standard deviation of the Gaussian distribution in depth. The standard deviation is related to the FWHM of a Gaussian distribution by FWHM = $2.355\ \Delta R_p$.

As a first approximation, ignoring any detector energy resolution and energy straggling issues, the range straggling ΔR_p is given by

$$\Delta R_p = \text{FWHM} / (2.355 N[\varepsilon_0]^{Si}_{As}) = 53.6\ \text{nm} \tag{5.39}$$

5.7 HIGH-ENERGY BACKSCATTERING AND THE ELASTIC RESONANCE OF 8.8 MEV HE WITH ^{16}O

Up to this point we have primarily concerned ourselves with backscattering experiments at relatively low energies. As discussed in Chapter 2, going to higher ion energies offers the advantage of producing greater mass separation in the backscattering spectra. However, it is well known that the likelihood for scattering to deviate from a Rutherford nature increases with increasing projectile energy (Figure 3.6). Deviations are expected when the projectile velocity is high enough to allow it to penetrate deep into the orbitals of the atomic electrons and interact with the nucleus of the target atom. Thus, if any sense is to be made of the information obtained from high-energy backscattering experiments, it will first be necessary to know the behavior for the scattering cross sections for all the elements involved.

A good example of where high-energy backscattering has been widely applied is in the compositional analysis of the thin film high-temperature superconductors $YBa_2Cu_3O_7$. A simulated 2 MeV $^4He^+$ RBS spectrum from a 400 nm thick $YBa_2Cu_3O_7$ film deposited on $SrTiO_3$ substrate is shown in Figure 5.8. Also shown in Figure 5.8 are simulated component backscattering signals from the individual elements existing in both film and substrate (Ba, Y, Cu, Sr, Ti, and O).

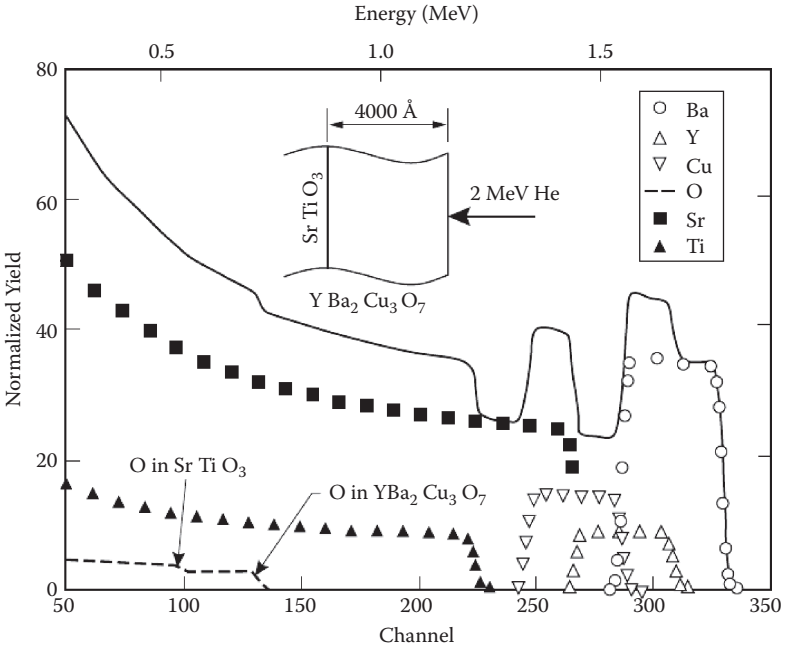

FIGURE 5.8 A simulated RBS spectrum of 2 MeV ^4He ions on a 400 nm thick $YBa_2Cu_3O_7$ film on a $SrTiO_3$ substrate. Also shown are the individual signals from Ba, Y, Cu, and O in the $YBa_2Cu_3O_7$ film and the signals from Sr, Ti, and O in the substrate.

Even without the substrate, there are considerable overlaps among Ba, Y, and Cu signals from the film. The complexity of adding the substrate greatly increases the difficulty of analyzing the oxygen concentration, because the oxygen signal will reside on the background of almost any substrate used in the synthesis of the high-temperature superconductors.

One way of increasing the separation between the heavy mass elements (Ba, Y, and Cu) and increasing the sensitivity to the oxygen is to perform experiments using the elastic resonance of 8.8 MeV He with ^{16}O. A typical backscattering spectrum for 8.8 MeV He incident on a 770 nm thick film of $YBa_2Cu_3O_7$ sitting on a $SrTiO_3$ substrate is shown in Figure 5.9. Indicated in the figure are the surface energies (KE_0) for Ba, Y, Cu, and O. The unlabeled step edges that appear at 2.80, 5.96, and 7.00 MeV correspond respectively to subsurface O, Ti, and Sr from the substrate. Clearly evident in these data is the good mass separation between Ba, Y, and Cu, as well as the large O yield from the superconductor film. However, the absolute accuracy for determining the film composition from such data depends on how well the scattering cross sections are known.

Thin film standards can be used to measure the ^4He scattering cross section as a function of energy. The first standard consisted of electron beam coevaporating a Y–Ba–Cu film onto a SiO_2 substrate that was capped with a Ti layer, which was used to determine the scattering cross-section ratios among Y, Ba, and Cu. The second standard consisted of evaporating Ba in the presence of O_2 onto a Ti-coated graphite substrate followed by another Ti cap layer, which was used to determine the scattering cross-section ratios between O and Ba. The substrates were chosen in each case because of their low kinematic factors.

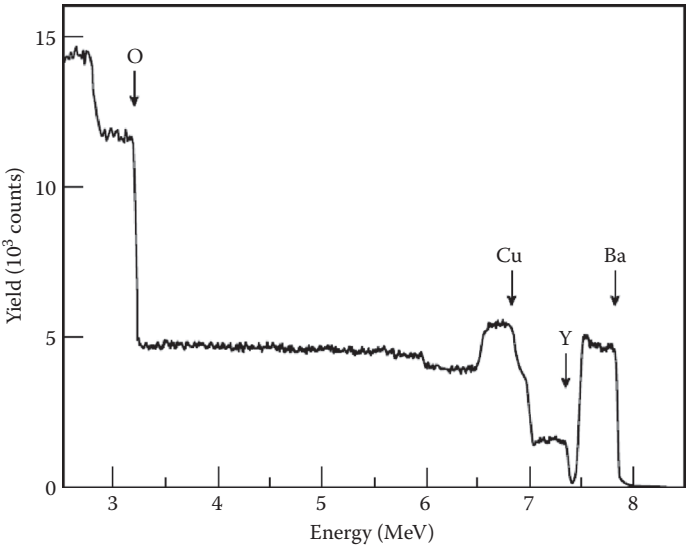

FIGURE 5.9 Typical backscattering spectrum for 8.8 MeV He ions incident on 770 nm thick film of $YBa_2Cu_3O_7$ on a $SrTiO_3$ substrate.

The Ti layers were employed to minimize environmental contamination and to aid in the adhesion to the graphite. For each standard, the film thickness was chosen to ensure elemental peak separation in a 2 MeV ^{4}He RBS spectrum. A schematic of the standard's structure and corresponding RBS spectra is shown in Figure 5.10.

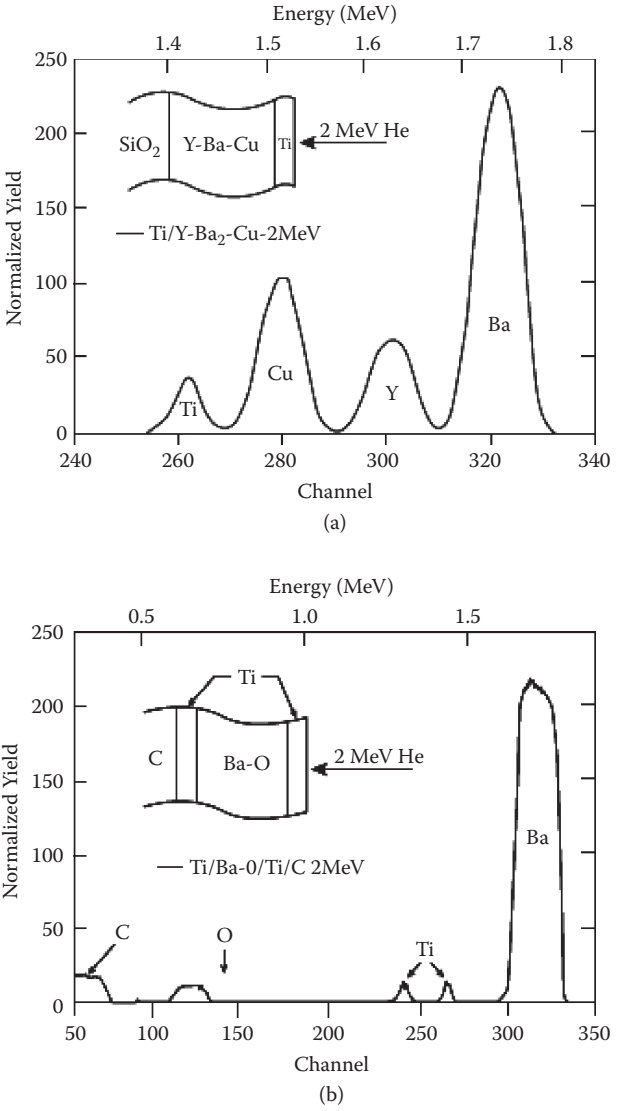

FIGURE 5.10 RBS data at 2 MeV from two reference film standards that were used to measure the relative cross sections of Cu, Y, and O relative to Ba as a function of He energy.

Performing peak integration on the data presented in Figure 5.10, applying Equation (5.27), and using the Rutherford cross section, the composition of Y and Cu relative to Ba (top spectrum) and O relative to Ba (bottom spectrum) was determined. Once the ratios of m/n are known (i.e., N_Y/N_{Ba}, N_{Cu}/N_{Ba}, N_O/N_{Ba}) at 2 MeV, where all the elements are Rutherford, Equation (5.27) can be inverted to measure the values of σ_A/σ_B at various energies by measuring the peak areas. For example, for σ_O/σ_{Ba} we have

$$\frac{\sigma_O(E)}{\sigma_{Ba}(E)} = \frac{N_O}{N_{Ba}} \frac{A_{Ba}}{A_O} \tag{5.40}$$

The results of this procedure for ^{4}He scattering from Ba and O in the energy range 8.2 to 9.1 MeV at $\theta = 166°$ are presented in Figure 5.11. Over this energy range, Ba is expected to have a Rutherford interaction with ^{4}He (see Figure 3.6). The dashed line at the bottom of the figure represents the ratio of cross sections assuming Rutherford scattering. The increase in sensitivity to ^{16}O at 8.8 MeV is about 32 times greater than for Rutherford scattering. The measured cross-section ratios for Y/Ba and Cu/Ba over the energy range 2 to 9 MeV are shown in Figure 5.12. The dashed line represents the Rutherford cross-section ratios. Assuming the scattering cross section for Ba remains Rutherford in this energy range, these data show that the Cu and Y cross sections start to deviate from Rutherford near 6.5 and 8.0 MeV, respectively.

With accurate cross-section data in hand, it is now possible to analyze the composition of a Y–Ba–Cu–O film from a backscattering spectrum taken with 8.8 MeV ^{4}He. A sample spectrum is presented in Figure 5.9. The analysis of these data will be left as a homework exercise.

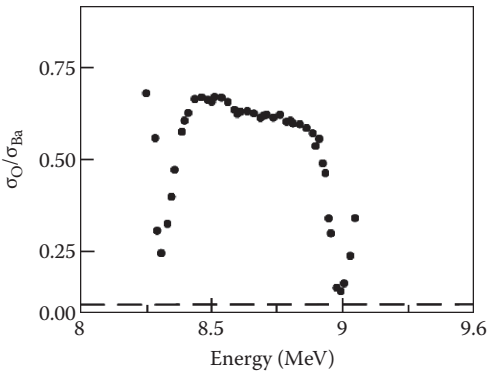

FIGURE 5.11 Ratio of scattering cross section for He ions scattering from ^{16}O and Ba as a function of He energy. The dashed line shows the ratio of the Rutherford scattering cross section.

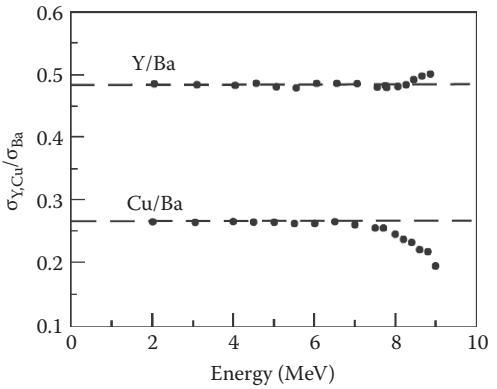

FIGURE 5.12 Ratios of scattering cross sections for He ions scattering from Y and Cu relative to Ba as a function of He energy. The dashed lines show the ratios of the Rutherford scattering cross sections.

PROBLEMS

5.1. Consider a 200 nm free-standing film of Pt with 2 MeV ^{4}He at normal incidence and the backscattering detector located at $\theta_2 = 10°$. For the backside of Pt at t = 200 nm, determine the following: (a) the value of E_1, (b) the value of ΔE_{in}, (c) the value of E_t, (d) the value of ΔE_S, (e) ΔE_{out}, and (f) the value of ΔE. Hint: Use the surface and mean energy approximations.

5.2. For the conditions listed in Problem 5.1, calculate [S] and [ε] using the surface and mean energy approximations. What is the percentage difference between these two approximations?

5.3. Consider a 200 nm film of Pt on a Si substrate with 2 MeV ^{4}He at an incidence of $\theta_1 = 10°$ and the backscattering detector located at $\theta_2 = 10°$. For the He scattering off of Si atoms at the interface, determine the following: (a) the value of E_1, (b) the value of ΔE_{in}, (c) the value of E_t, (d) the value of ΔE_S, (e) ΔE_{out}, and (f) the value of ΔE. Hint: Use the surface and mean energy approximations.

5.4. For the conditions listed in Problem 5.3, calculate [S] and [ε] using the surface and mean energy approximations. What is the percentage difference between these two approximations?

5.5. Consider a 100 nm free-standing film of Ni_2Si (mass density of 7.23 g/cm^3) with 2 MeV ^{4}He at normal incidence and the backscattering

detector located at $\theta_2 = 10°$. (a) What is the value of N^{Ni_2Si}? (b) What is the value of $\varepsilon_{in}^{Ni_2Si}$? (c) What is the value of $[\varepsilon]_{Ni}^{Ni_2Si}$? (d) What is the value of $[\varepsilon]_{Si}^{Ni_2Si}$ using the surface energy approximation?

5.6. Consider the following experimental conditions to measure Pt thin film on Si substrate: 3 MeV $^4He^{++}$, $\theta_1 = 60°$, $\theta = 170°$, $\xi = 2.5$ keV, $\Omega = 4$ msr, and $Q = 20$ μC. (a) How many He ions are there bombarding the sample? (b) If the average particle current during the experiment is 20 nA, how long did it take to acquire the spectrum? (c) How many counts would you expect in a Pt peak from a 10 nm thick Pt film with this measurement? (d) What is the Si surface height?

5.7. Using a ruler, measure the relative surface heights of Ba, Y, Cu, and O in the Y–Ba–Cu–O backscattering spectrum shown in Figure 5.9. Using these values, together with the cross section data in Figures 5.11 and 5.12, estimate N_Y/N_{Ba}, N_{Cu}/N_{Ba}, and N_O/N_{Ba}. Compare them to scattering cross section values obtained from data in Figure 5.8.

5.8. 2 MeV ^{4}He particles are scattered off a thin foil of an elemental material with atomic number Z_1, mass density ρ_1, mass number A_1, and thickness t_1. The backscattering spectrum was collected at the scattering angle θ, solid angle Ω, and accumulated charge Q, which yield the peak area of Y_1. (a) If the foil is replaced with another thin foil of different elements (Z_2, ρ_2, A_2, and t_2), what is the expected peak area of Y_2 for the new foil, assuming Rutherford cross sections for both foils? (b) If the foil is 10 μg/cm^2 of Au, what fraction of the incident He particles will be backscattered at $\theta = 150°$ into a detector with cone of the solid angle 5 msr? (c) If the foil is 10 μg/cm^2 of Au, what fraction of the incident He particles will be backscattered forward scattered at $\theta = 30°$ into a detector with $\Omega = 5$ msr?

5.9. For Problem 5.8, what fraction of incident He particles is backscattered from the free-standing Au foil (e.g., $\theta > 90°$)?

5.10. Assume in backscattering measurements that energy straggling is given by $\Omega_{tot}^2 = (K\Omega_{B,in})^2 + \Omega_{B,out}^2$. Calculate the amount of energy straggling in an RBS signal from a ultrathin Au layer underneath an Ag film of 400 nm thick with an analysis beam of 2 MeV ^{4}He ions at $\theta = 180°$? What is the total Au signal width (FWHM) if the detector resolution is 15 keV? What thickness of Ag does this correspond to?

REFERENCES

Chu, W.-K., Mayer, J. W., and Nicolet, M.-A. 1978. *Backscattering spectrometry,* chap. 2. New York: Academic Press.

SUGGESTED READING

Alford, T. L., Feldman, L. C., and Mayer, J. W. 2007. *Fundamentals of nanoscale film analyses.* New York: Springer.

Wang, Y., and M. Nastasi, eds. 2009. In *Handbook of modern ion beam materials analysis,* 2nd ed., chap. 4. Warrendale, PA: Materials Research Society.